NASA
Technical
Paper
2505

November 1985

Location of Noise Sources Using a Phase-Slope Method

Richard DeLoach and
John S. Preisser

NASA

NASA Technical Paper 2505

1985

Location of Noise Sources Using a Phase-Slope Method

Richard DeLoach and
John S. Preisser

Langley Research Center
Hampton, Virginia

NASA
National Aeronautics
and Space Administration

**Scientific and Technical
Information Branch**

SUMMARY

A laboratory experiment has been conducted in which acoustic signals propagating over both anechoic and reflective surfaces were detected by a pair of three-element microphone arrays. The phase component of the cross power spectrum between array elements has been examined for both ground impedance cases with the source location inferred from the slope of the phase spectra. The effect of ground reflections on both the accuracy and precision of position estimates made in this way is examined.

INTRODUCTION

The use of sensor arrays for the detection and localization of an acoustic-emitting source has found application in several fields. Sensors mounted on the surface of a material under stress have been used to detect acoustic emissions from a defect within the material (ref. 1). A multimicrophone acoustic ranging technique has been used to assess the degree of concentration of noise generated by the rotating blades of a wind turbine (ref. 2). Cross-correlation techniques between several pairs of microphones were employed to measure the sound radiated by a wing/flap configuration in a wind tunnel (ref. 3). Various applications generally make use of either correlation techniques for estimating time delay between array elements or phase information for the purpose of determining the direction of a coherent wave front as it passes the array. In general, the goal of either method has been to minimize the random error in the intersensor time delay (or phase difference) in the presence of statistically independent noise at the array locations. It is usually assumed that dispersion of the estimates about their mean is due only to statistical sampling errors. In most applications, however, errors occur because of factors other than sampling considerations, such as wind and thermal refraction, scattering by objects or atmospheric inhomogeneities, and reflections from boundaries.

The present report describes a simple approach used to locate an acoustic source passively and presents some accompanying experimental data to demonstrate its use under optimal conditions. The approach makes use of a linear best-fit regression to the slope of the phase-frequency plots between array elements. It was shown in reference 4 that phase data regression lines yield results with the same accuracy as other optimal time-delay estimation procedures. Moreover, phase data have an advantage in that extraneous noise sources having a different frequency content can be distinguished, and systematic errors can be assessed from the knowledge that the phase should be 0 for infinite wavelengths.

The present analysis is for the case of two three-element microphone arrays. Tests to demonstrate the technique were performed in an anechoic facility in order to control meteorological and, hence, propagation effects. The objective was to establish statistical bounds on range, elevation, and azimuth for a stationary source under optimum test conditions. Results are presented for both pure-tone and broadband noise. Several source positions were tested in order to assess the effect of elevation angle on source localization. The effect of simulating extreme changes in boundary impedance on the ability to localize a source in space confidently is also addressed.

SYMBOLS

Values are usually given in SI Units but, where considered useful or expedient, are also given in U.S. Customary Units. Measurements and calculations were made in U.S. Customary Units.

c	speed of sound, m/sec
c_o	speed of sound at temperature T_o, m/sec
c_{xy}	phase speed in direction of line joining microphone positions x and y, m/sec
f	acoustic frequency, Hz
$\vec{k}$	wave number vector, m^{-1}
k_{xy}	component of wave number vector in direction defined by microphone positions x and y, m^{-1}
m_{xy}	slope of phase-frequency function (where phase is measured between microphones at positions x and y)
r	range (distance from source to reference microphone), m
r_I	distance from source to reference microphone in array I, m (ft)
r_{II}	distance from source to reference microphone in array II, m (ft)
s	separation distance between microphone arrays, m
T	ambient temperature, K
T_o	reference temperature, K
θ	source elevation angle, relative to plane of microphone array, deg
θ_I	elevation angle of source from array I, deg
θ_{II}	elevation angle of source from array II, deg
ξ	microphone separation, m
ϕ_{xy}	phase difference between signals measured at microphone positions x and y
ψ	source azimuthal angle with respect to microphone array, deg
ψ_I	azimuthal angle to source from array I, deg
ψ_{II}	azimuthal angle to source from array II, deg

THEORY

Assume that an acoustic wave of frequency f is propagating from a source located at spherical coordinates r, θ, and ψ relative to the origin of a coordinate system, where r is the distance to the source, θ is an elevation angle, and ψ is an azimuthal angle. (See fig. 1.)

Assume further that a three-element microphone array is located in the $\theta = 0°$ plane of this frame of reference, with one microphone (microphone B) located at the origin and the other two (microphones A and C) located at $r = \xi$, $\psi = 0°$ and at $r = \xi$, $\psi = \pi/2$, as shown in figure 2.

If $\xi/r << 1$, the wave front curvature may be ignored. The component of the wave number vector in the $\theta = 0°$ plane can be resolved into two orthogonal components, k_{BA} and k_{BC}, which correspond to the $\psi = 0°$ and $\psi = \pi/2$ directions, respectively. The difference in phase between signals received at microphones B and A, ϕ_{BA}, is just $k_{BA}\xi$ for $k_{BA}\xi \leq 2\pi$. Similarly, $\phi_{BC} = k_{BC}\xi$ for $k_{BC}\xi \leq 2\pi$. The two phase differences can be expressed in terms of frequency as follows:

$$\phi_{BA} = \frac{2\pi\xi f}{c_{BA}} \tag{1a}$$

$$\phi_{BC} = \frac{2\pi\xi f}{c_{BC}} \tag{1b}$$

where c_{BA} and c_{BC} are phase speeds in the $\theta = 0°$, $\psi = \pi/2$ and $\theta = 0°$, $\psi = 0°$ directions, respectively.

Let m_{BA} and m_{BC} be the derivatives of ϕ_{BA} and ϕ_{BC}, respectively, with respect to frequency. Then,

$$m_{BA} = \frac{2\pi\xi}{c_{BA}} = \frac{\xi k_{BA}}{f} \tag{2a}$$

$$m_{BC} = \frac{2\pi\xi}{c_{BC}} = \frac{\xi k_{BC}}{f} \tag{2b}$$

Neglecting effects such as refraction, which may cause the ray paths to bend, the azimuthal angle ψ is

$$\psi = \tan^{-1}\frac{k_{BC}}{k_{BA}} \tag{3}$$

or

$$\psi = \tan^{-1} \frac{m_{BC}}{m_{BA}} \tag{4}$$

and the elevation angle θ is

$$\theta = \cos^{-1} \sqrt{\frac{k_{BA}^2 + k_{BC}^2}{k}} \tag{5}$$

From equations (2),

$$k_{BA} = \frac{m_{BA} f}{\xi} \tag{6a}$$

$$k_{BC} = \frac{m_{BC} f}{\xi} \tag{6b}$$

Inserting equations (6) into (5) gives

$$\theta = \cos^{-1} \frac{f}{\xi k} \sqrt{m_{BA}^2 + m_{BC}^2} \tag{7}$$

or

$$\theta = \cos^{-1} \frac{c}{2\pi\xi} \sqrt{m_{BA}^2 + m_{BC}^2} \tag{8}$$

where c, the speed of sound, depends on ambient temperature T as follows:

$$c = c_o \sqrt{\frac{T}{T_o}} \tag{9}$$

where c_o is the speed of sound at temperature T_o. Insert equation (9) into (8) to express the temperature dependence of θ:

$$\theta = \cos^{-1} \frac{c_o}{2\pi\xi} \sqrt{\left(m_{BA}^2 + m_{BC}^2\right)\frac{T}{T_o}} \tag{10}$$

The bearing angles θ and ψ must be known at two different locations to determine the range to the source by triangulation. Assume a geometry as in figure 3 in which two triangular arrays similar to that illustrated in figure 2 are located in the $\theta = 0°$ plane. Array I contains microphones A, B, and C and array II contains microphones D, E, and F. Let the subscripts I and II refer to measurements made with respect to arrays I and II, respectively, and let s be the separation distance between microphones B and E, as shown in figure 3. Then,

$$r_I = \frac{s \sin \psi_{II}}{\cos \theta_I \sin(\psi_I + \psi_{II})} \tag{11a}$$

and

$$r_{II} = \frac{s \sin \psi_I}{\cos \theta_{II} \sin(\psi_I + \psi_{II})} \tag{11b}$$

Equations (4), (10), and (11) can be used to predict the location of a noise source from an analysis of relative phase spectra. Equations (1) indicate that the phase difference between signals received at two adjacent microphones in the array of figure 2 is directly proportional to frequency. Regression analysis on the phase spectra for microphone A relative to B and for microphone C relative to B will yield the slope values m_{BA} and m_{BC}, respectively, used to calculate bearing angles via equations (4) and (10). Bearing angles computed in the same way for a second array can be used to calculate range values as in equations (11).

TEST DESCRIPTION

Test Setup

The microphone array geometry of figure 3 was established in the Langley Anechoic Noise Facility (fig. 4). Each array consisted of three 1/2-in. condenser microphones defining an isosceles right triangle, with the microphones that defined the equal legs of the triangle separated by a distance of 0.1 m (fig. 5). The microphone at the 90° corner of each array was defined as the reference microphone in that array, and all source locations were measured with respect to the center of the reference microphone diaphragm.

The plane of each array was located 1.79 m above the floor of the anechoic chamber. Covering the floor were polyurethane foam wedges 0.91 m in height, so that the plane of each microphone array was 0.88 m above the tips of the wedges. The spacing between the tips of the wedges varied from 0.3 to 0.4 m. An anechoic wedge treatment also covered the walls and ceiling of the chamber. The two arrays were separated by a distance of 5.26 m between reference microphones. Each array was located approximately 1.5 m from the sidewall wedge tips.

A small acoustic driver, fitted with a tapered flange, was used as a point source of noise (fig. 6). Four source positions were selected, as shown in table I. These source positions were determined relative to the reference microphone in each array by using a theodolite. The theodolite measurements are assumed to represent the true source location.

TABLE I.- NOISE SOURCE POSITIONS

Noise source		Array I			Array II		
No.	Position	r_I, m (ft)	ϕ_I, deg	ψ_I, deg	r_{II}, m (ft)	ϕ_{II}, deg	ψ_{II}, deg
1	High, center	7.3 (23.9)	40.5	62.0	7.3 (23.9)	40.5	62.0
2	Low, side	4.8 (15.8)	7.3	83.2	6.7 (21.9)	5.2	45.5
3	High, side	7.2 (23.6)	42.0	86.7	8.7 (28.5)	33.6	47.4
4	Low, center	5.0 (16.4)	6.7	58.7	5.0 (16.5)	6.4	58.2

The microphones were removed from their mounting hardware during theodolite measurements, and a specially designed theodolite mount was used to ensure that all measurements were made with respect to the position of the reference microphone diaphragm (fig. 7).

Test Conditions

Ten discrete frequencies were broadcast at each of the four noise source positions in table I. The frequencies ranged from 200 to 2000 Hz in 200-Hz increments, with the lower frequency dictated by the performance of the chamber (not anechoic at frequencies substantially below 200 Hz) and the upper frequency based on the microphone array geometry. (Wavelengths were chosen to be larger than the microphone spacing to ensure coherence.) In addition to the 10 pure tones, white noise in the range from 200 to 2000 Hz was broadcast at each source position. For each combination of source position and frequency, data were acquired for a "soft floor" and a "hard floor" to simulate data acquisition under significantly different ground impedance conditions. The soft floor was achieved by leaving the anechoic foam rubber floor wedges in place, as shown in figure 4. For the hard-floor measurements, the floor wedges were removed, exposing a rigid plywood surface.

Data Acquisition

Prior to the primary data-acquisition activity, a preliminary set of measurements was made to determine the phase characteristics of each microphone. The phase response of each microphone was compared with a reference microphone at each of the discrete-tone test frequencies. Differences in these phase responses for each microphone pair, which were averaged over the 10 pure-tone test frequencies, are presented in table II. These phase differences are small and were ignored in the test.

TABLE II.- AVERAGE PHASE DIFFERENCE FOR EACH MICROPHONE PAIR

Microphone pair	Average phase deviation, deg	Standard deviation, deg
B,A	0.3	$\pm$0.5
B,C	.4	$\pm$.4
E,D	.7	$\pm$.8
E,F	1.1	$\pm$1.0

During the pure-tone measurements, a narrow-band analyzer was used to measure the amplitude and phase components of the cross power spectra for all three unique combinations of microphone pairs in each array. A sample rate of 8192 Hz and a bandwidth of 4000 Hz were used in these measurements. The amplitude spectra were discarded because only phase information is required to determine source position by the method of this paper. For the pure-tone measurements, only the one point in the phase spectrum corresponding to measurement frequency was meaningful, and the phase at that frequency was recorded for subsequent analysis. The broadband data were acquired in a manner similar to that of the pure-tone data, except that the entire phase spectrum in the range from 200 to 2000 Hz was recorded for subsequent analysis.

RESULTS AND DISCUSSION

For each combination of source position and ground impedance (four positions by two impedance conditions, resulting in eight cases altogether), phase differences were plotted against frequency for microphone pairs B,A, B,C, E,D, and E,F. This process was repeated for both the pure-tone and the broadband cases. Figures 8 and 9 are the phase spectra corresponding to the soft-floor measurements of source position 1 (see table I) for the pure-tone and broadband measurements, respectively, whereas figures 10 and 11 are the corresponding phase spectra for the hard-floor case. These spectra are representative of the phase data acquired at the other three source positions. The hard-floor spectra deviate more from the theoretical straight line predicted by equations (1) than the soft-floor data, a result that is believed to be due to the influence of the hard-floor reflections on the phase measurements. Such reflections would cause signal cancellations and additions, depending on frequency, with a corresponding distortion in the phase spectra as seen in the data. Despite some fluctuations, all eight combinations of source position and floor impedance gave phase spectra that were well represented by a linear fit, as represented by

the straight lines in figures 10 and 11. Linear-regression correlation coefficients for the pure-tone data, averaged over the four microphone pairs, are displayed in figure 12 for each combination of source position and ground impedance. The average correlation coefficients ranged from 0.83 to 0.96 for the hard-floor data and from 0.92 to 0.99 for the soft-floor data, where a value of 1.00 would correspond to the theoretical prediction of equations (1). These results further suggest that source location errors are greater in the presence of reflections from a hard surface than from a soft surface.

Accuracy of Acoustic Measurements

The slope of the best straight-line fit for each phase spectrum was used in equations (4) and (10) to compute bearing angles to the source from the corner microphone of each array. These bearing angles were then used in equations (11) to compute the distance to the source. Figures 13 and 14 compare the hard-floor and soft-floor measurements of range, elevation angle, and azimuthal angle for arrays I and II, obtained from the pure-tone acoustic data, with the corresponding coordinates of table I, obtained by theodolite measurements. Figures 15 and 16 make similar comparisons between the broadband acoustic measurements and the theodolite measurements.

The following observations can be made from the data in figures 13 to 16. The agreement between acoustic and theodolite measurements of range and bearing angles is better for the soft-floor case than for the hard-floor case. It is suspected that ground reflections contaminated the phase measurements that were used to forecast the source location. There was better agreement between acoustic data and theodolite measurements for the broadband data than for the pure-tone data, a result attributed to the more complete statistics resulting from the greater number of data points used in the broadband regression analysis (205 for the broadband data against 10 for the pure-tone data). The extent to which the broadband data improved the estimate of source position was greater for the hard-floor data than for the soft-floor data, and it was greater for the two lower elevation angles than for the two higher elevation angles. This again indicates the effects on phase measurements that hard-floor ground reflections had when compared with the reduced soft-floor ground reflections.

The results of figures 13 to 16 are condensed in figure 17, which compares source locations measured from the acoustic data with source locations measured by theodolite. The comparisons are made in terms of the distance between source locations measured acoustically and by theodolite. Figure 17(a) presents the results for the pure-tone data, and figure 17(b) presents the results for the broadband data. Again, there is better agreement with soft-floor measurements than with hard-floor measurements. The theodolite measurements agree better with the broadband acoustic results than with the sparser pure-tone data, with the extent of improvement greater for the hard-floor cases than for the soft-floor cases.

Precision of Acoustic Measurements

The upper and lower limits on the 90-percent confidence intervals for each slope estimate were computed during the regression analysis that fit the best straight line to the phase spectra of figures 8 and 9. Similar confidence intervals were computed for the other source positions. Equations (4), (10), and (11) were then used to transform these slope confidence intervals into confidence intervals in r, θ, and ψ. The upper and lower limits on these spherical-coordinate confidence inter-

vals were converted to rectangular coordinates and plotted in figure 18 relative to the source position determined from theodolite measurements. Figures 18(a) and (b) correspond to one of the source locations and, for each figure, the 90-percent confidence intervals are represented as rectangles that define the 90-percent confidence regions in rectangular coordinate space. These 90-percent confidence regions are plotted for both the hard-floor and soft-floor data. Each figure illustrates both the horizontal plane and the vertical plane of the 90-percent confidence region. Also plotted in these figures are the hard-floor and soft-floor estimates of the source position.

The magnitude of source position errors has been discussed earlier in this report. Figure 18 illustrates the direction of these errors as well as their magnitudes. Figure 18 also graphically represents the precision with which source position estimates were made in these tests; it can be said with 90-percent confidence that the actual source position lies within the regions depicted in these figures.

Note that the 90-percent confidence regions are smaller for the soft-floor data than for the hard-floor data, again indicating the effect of ground reflections on the precision with which an acoustic source can be located by the phase-slope method. The degree of reduction in the size of the confidence intervals going from the hard floor to the soft floor is greater at lower elevation angles than at higher elevation angles, a fact that is attributed to the greater effect of ground impedance and lower elevation angles.

The 90-percent confidence intervals tend to be wider on the elevation angles than on the azimuthal angles, as indicated by the somewhat vertically elongated shapes of the confidence regions in figure 18. This result is attributed to the rather strong vertical temperature gradient that existed in the anechoic chamber during the noise measurements (typically 0.3°C per meter). This gradient is likely to have caused refraction effects that may have adversely affected the elevation angle measurements. A strong vertical temperature gradient would tend to bias the elevation angle measurements higher, a phenomenon that would be offset to some extent by the effect of ground reflections, which would bias the elevation angle estimates lower. Evidence of the temperature effect can be seen in figure 18 in which the 90-percent confidence intervals in the vertical direction are generally larger for the higher elevation angles (for which the temperature variations are greatest) than for the lower elevation angles (for which the temperature variations are less over the propagation path).

Bearing angles can be computed on the basis of phase information obtained at a single frequency, but the phase-slope method described in this paper offers significant advantages over such single-point measurements because phase information obtained simultaneously at several frequencies is used in the computations. Random distortions in the phase spectrum, caused by such factors as meteorological effects, reflections, and ambient noise, are manifested as positive and negative excursions about the best straight-line fit to the phase spectrum. Even spectra with relatively large fluctuations about the theoretical straight-line fit predicted by equations (1) can forecast bearing angles well, as long as such fluctuations are random in nature and do not systematically bias the slope of the phase spectrum in one direction or another, as illustrated by figure 11. These phase spectra were acquired under the relatively unfavorable condition of a high-impedance (rigid plywood) reflecting floor, with ground reflections interfering with the primary source signals to produce the distortions seen in these phase spectra. Since these distortions are more or less randomly distributed about the best straight-line fit, the corresponding regression values still result in relatively good bearing angle forecasts, although some-

what degraded from the anechoic floor case. These results suggest that the phase-slope method described here may be less sensitive to the large random fluctuations that characterize single-point phase measurements under imperfect propagation conditions that are customarily encountered outdoors.

CONCLUDING REMARKS

A phase-slope method using two three-element microphone arrays has been used to predict the position of both pure-tone and broadband noise sources in an anechoic chamber. A methodology for quantitatively assessing both the accuracy and precision of such a source location technique has been introduced and illustrated. The effects of a change in ground impedance on the accuracy and precision with which a noise source can be located acoustically were investigated. When the phase-slope method was used, there was higher accuracy and more precision in estimates of source location with a small ground impedance than with a large ground impedance. Ground impedance effects were observed to be larger for low elevation angles than for high elevation angles.

NASA Langley Research Center
Hampton, VA 23665-5225
August 19, 1985

REFERENCES

1. Tobias, A.: Acoustic-Emission Source Location in Two Dimensions by an Array of Three Sensors. Non-Destruct. Test., vol. 9, no. 1, Feb. 1976, pp. 9-12.

2. Kelley, N.: Acoustic Ranging Technique for Assessing Low-Frequency Acoustic Noise From Wind Turbines. Wind Eng., vol. 8, no. 1, 1984, pp. 19-22.

3. Miller, Wendell R.; Meecham, William C.; and Ahtye, Warren F.: Large Scale Model Measurements of Airframe Noise Using Cross-Correlation Techniques. J. Acoust. Soc. America, vol. 71, no. 3, Mar. 1982, pp. 591-599.

4. Piersol, Allan G.: Time Delay Estimation Using Phase Data. IEEE Trans. Acoust., Speed, & Signal Process., vol. ASSP-29, no. 3, June 1981, pp. 471-477.

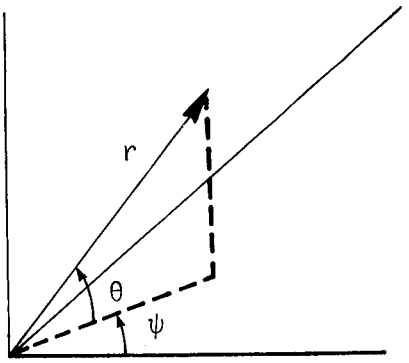

Figure 1.- Coordinates of source.

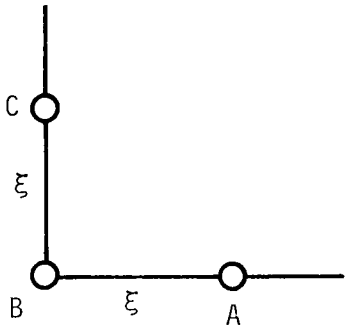

Figure 2.- Microphone configuration.

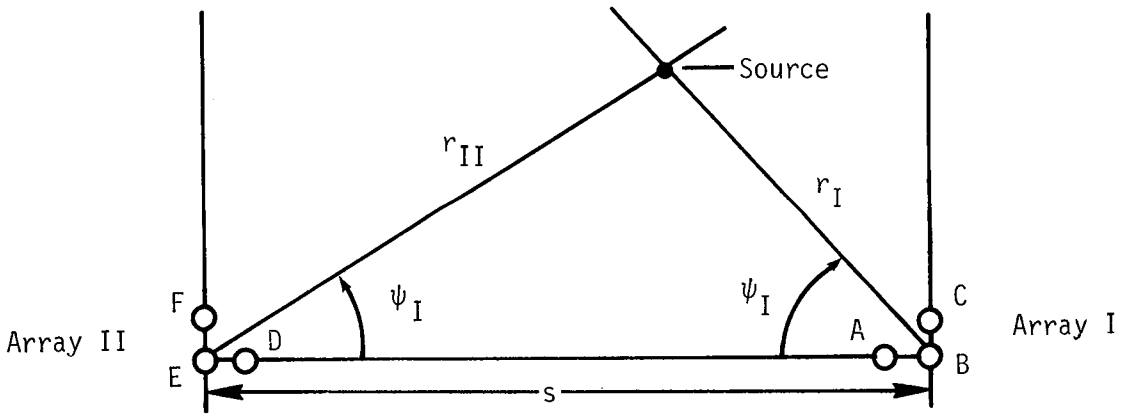

Figure 3.- Array geometry viewed from top.

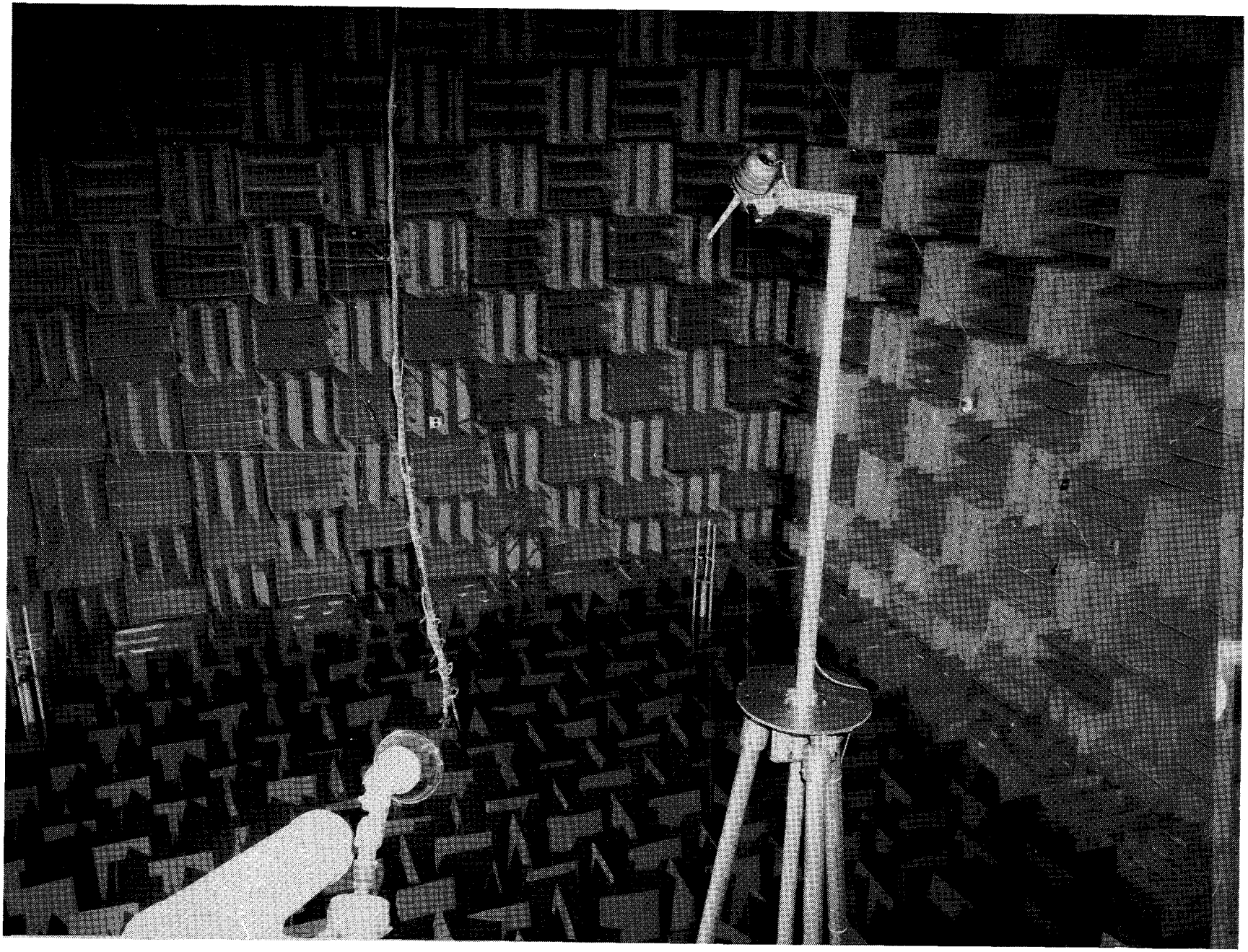

Figure 4.- Anechoic chamber with source and arrays.

L-83-9217

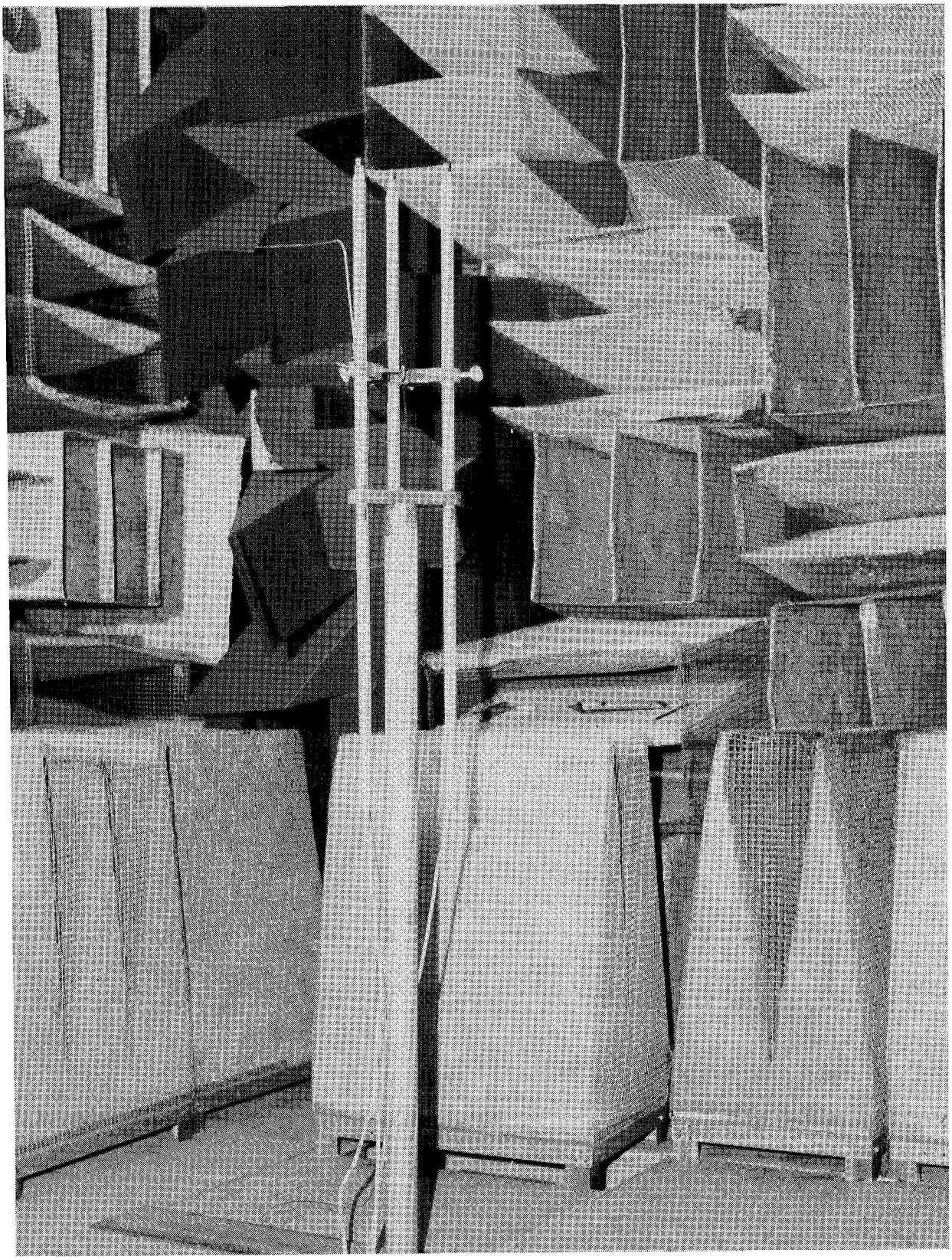

L-83-9210

Figure 5.- Microphone array.

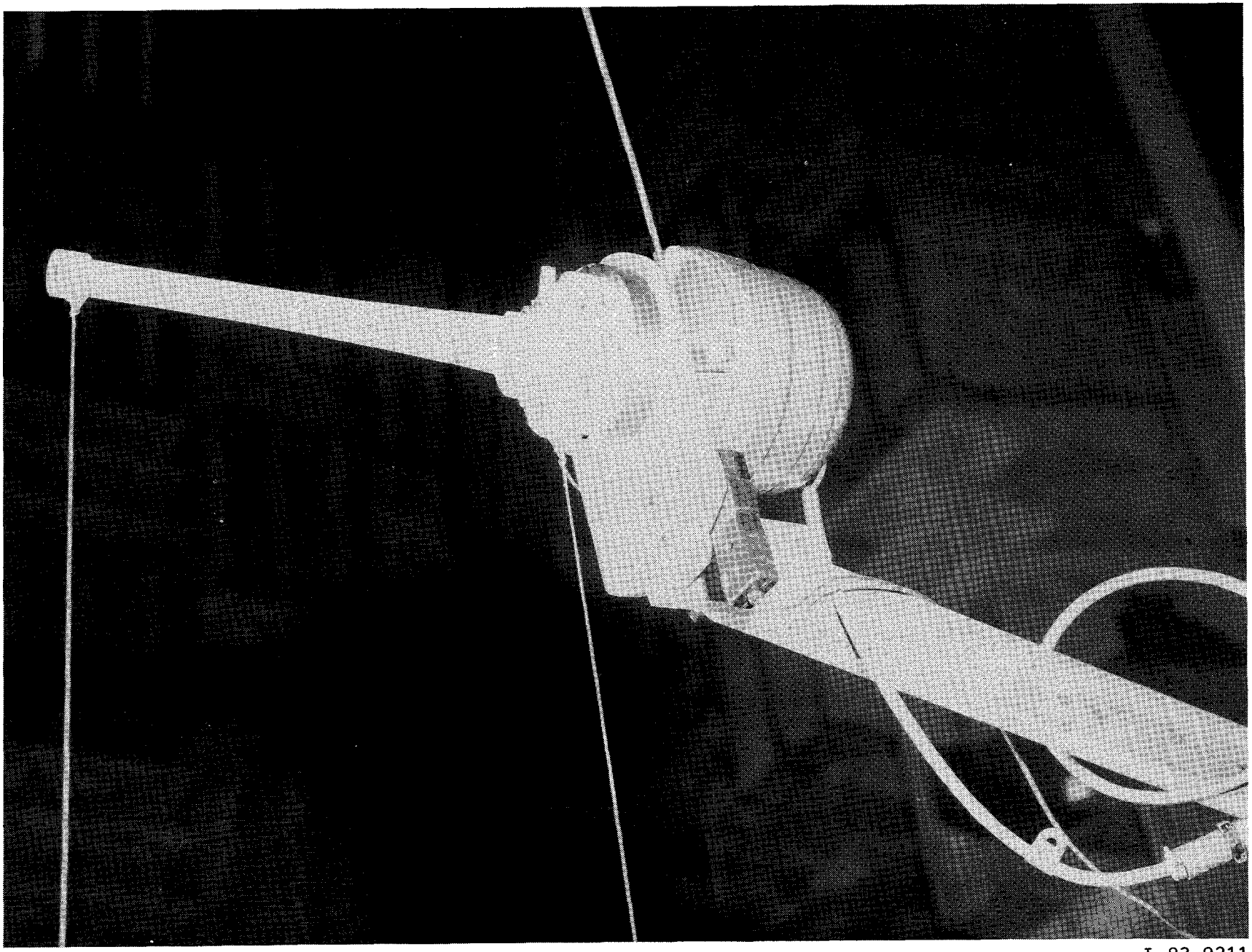

L-83-9211

Figure 6.- Noise source.

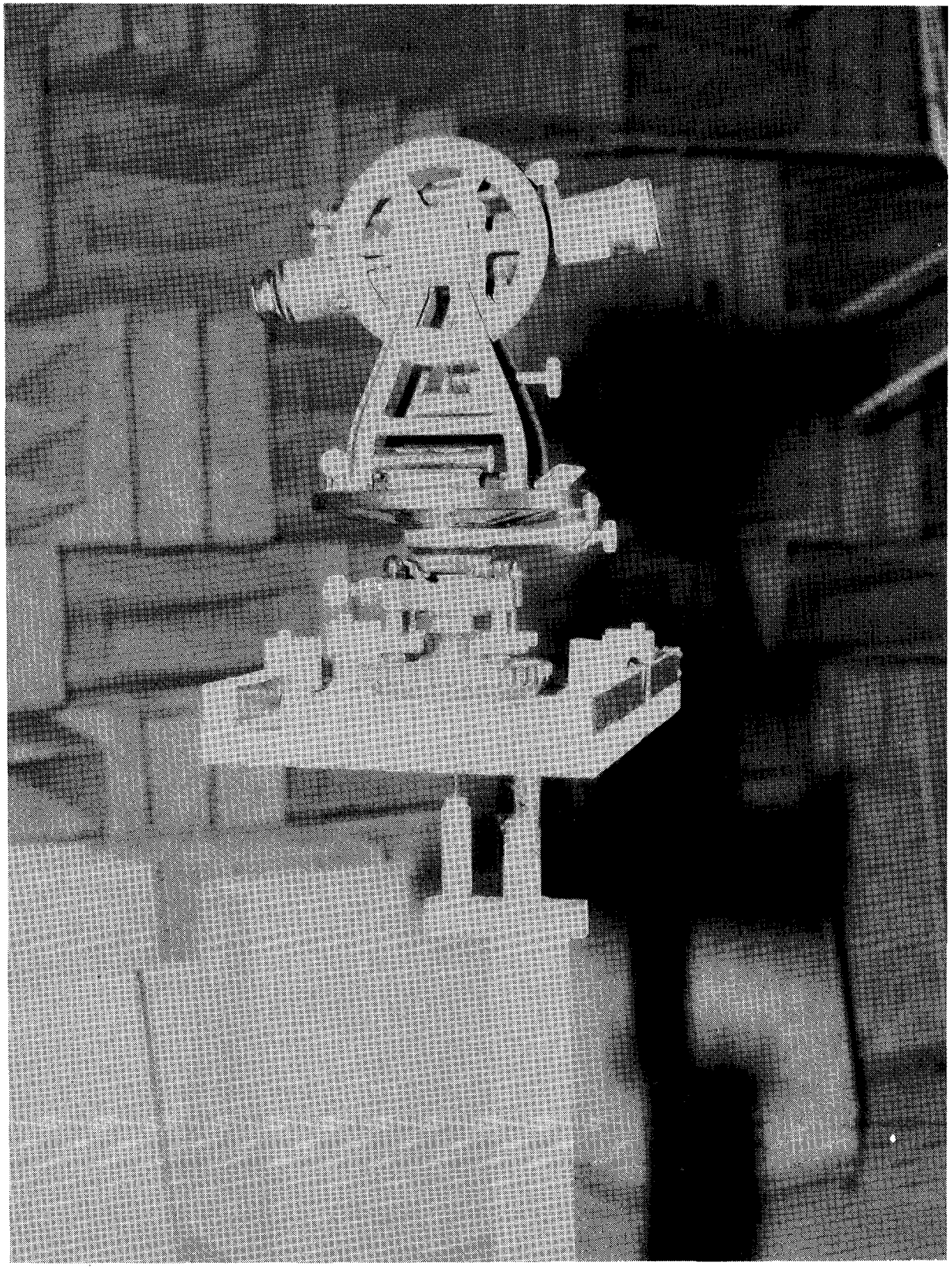

L-83-9214

Figure 7.- Apparatus measuring source position.

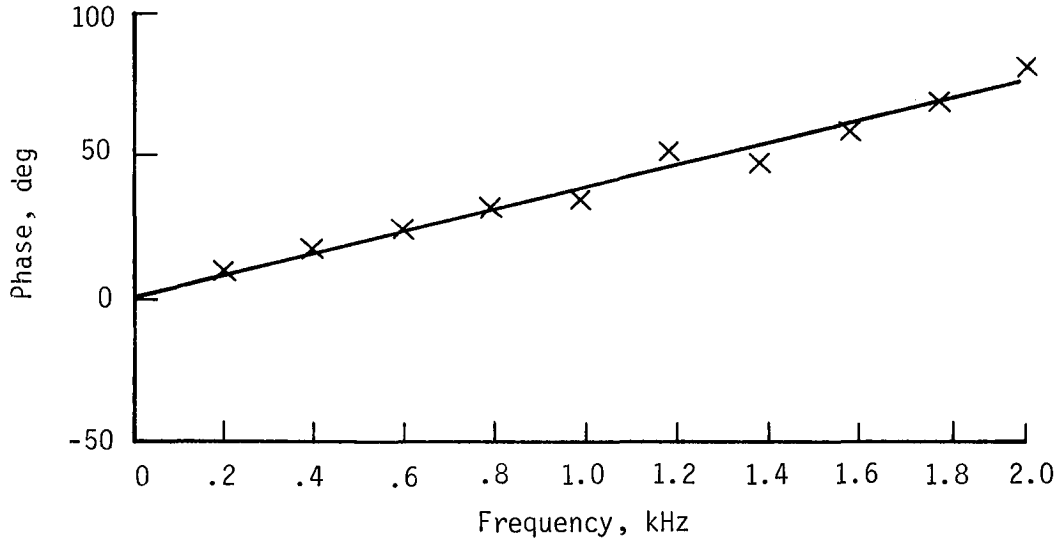

(a) Microphone pair B,A.

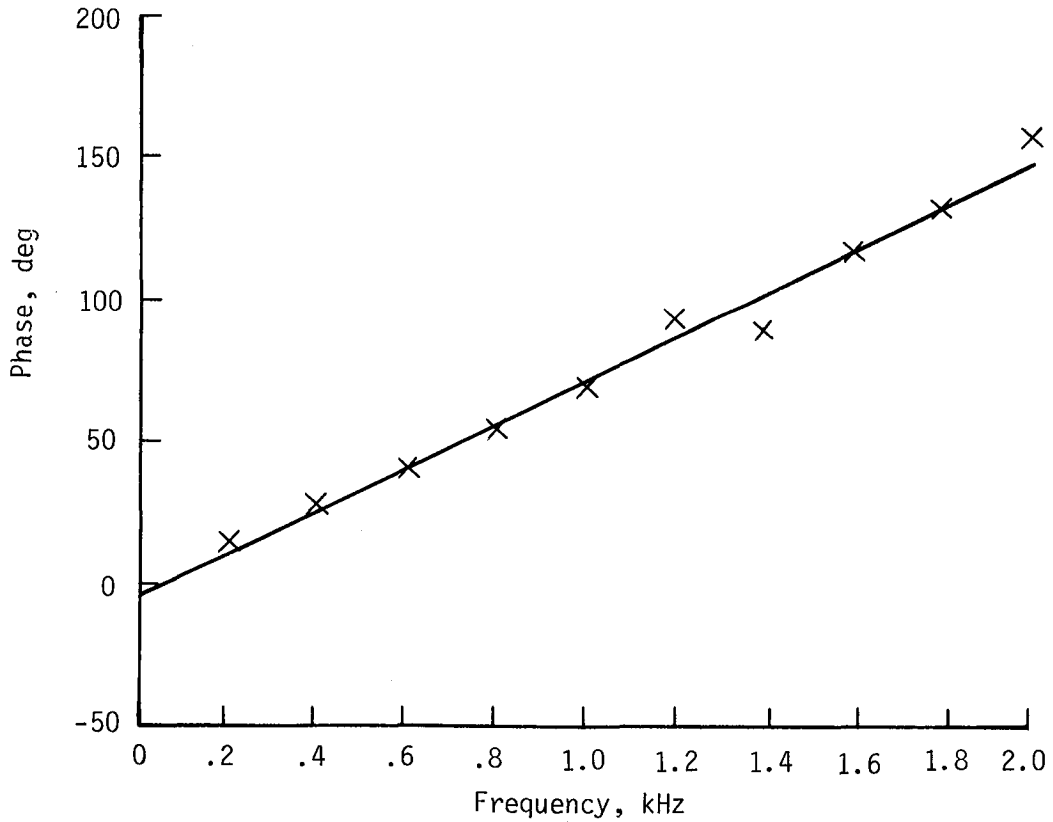

(b) Microphone pair B,C.

Figure 8.- Phase spectrum corresponding to soft-floor measurements of source position 1 for pure-tone measurements.

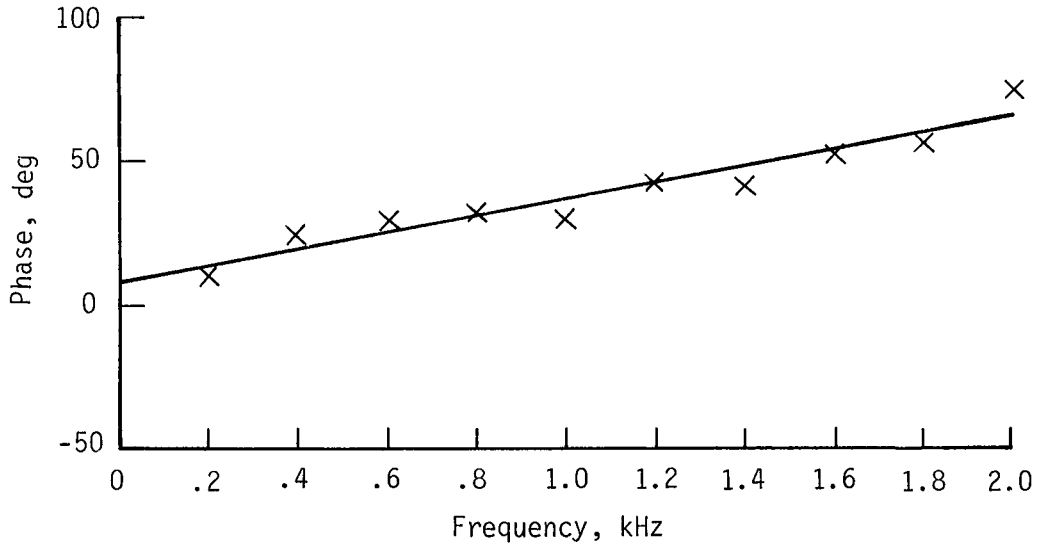

(c) Microphone pair E,D.

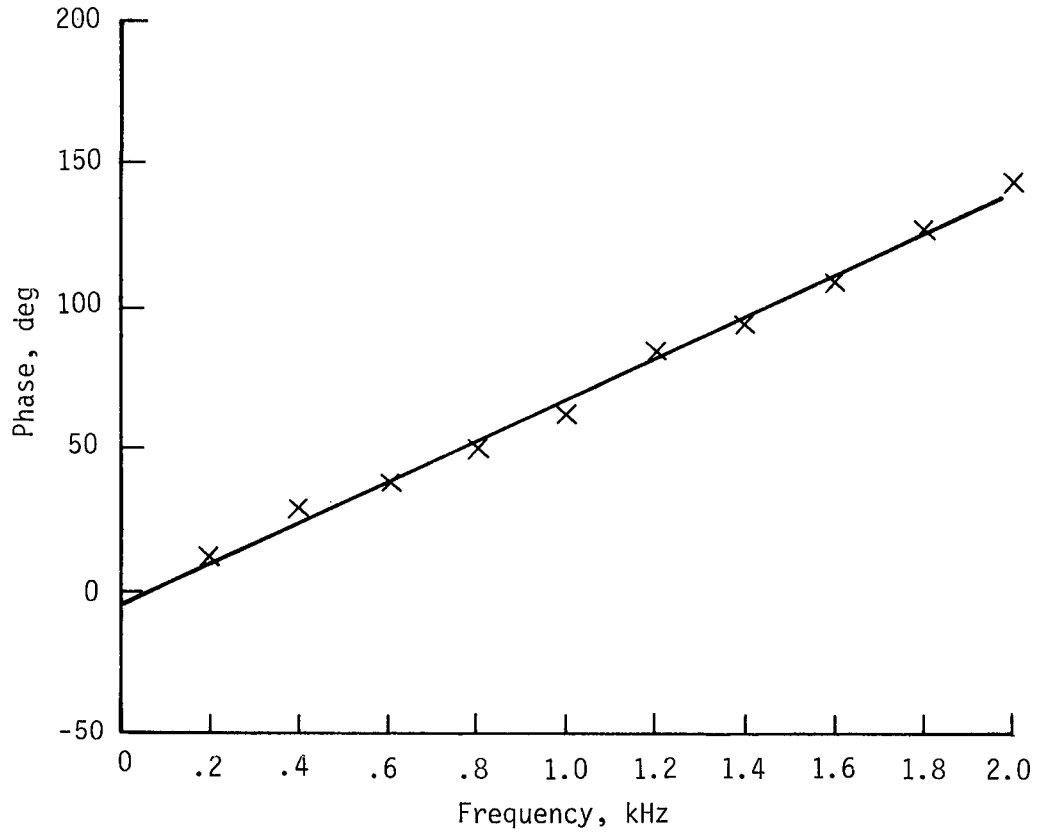

(d) Microphone pair E,F.

Figure 8.- Concluded.

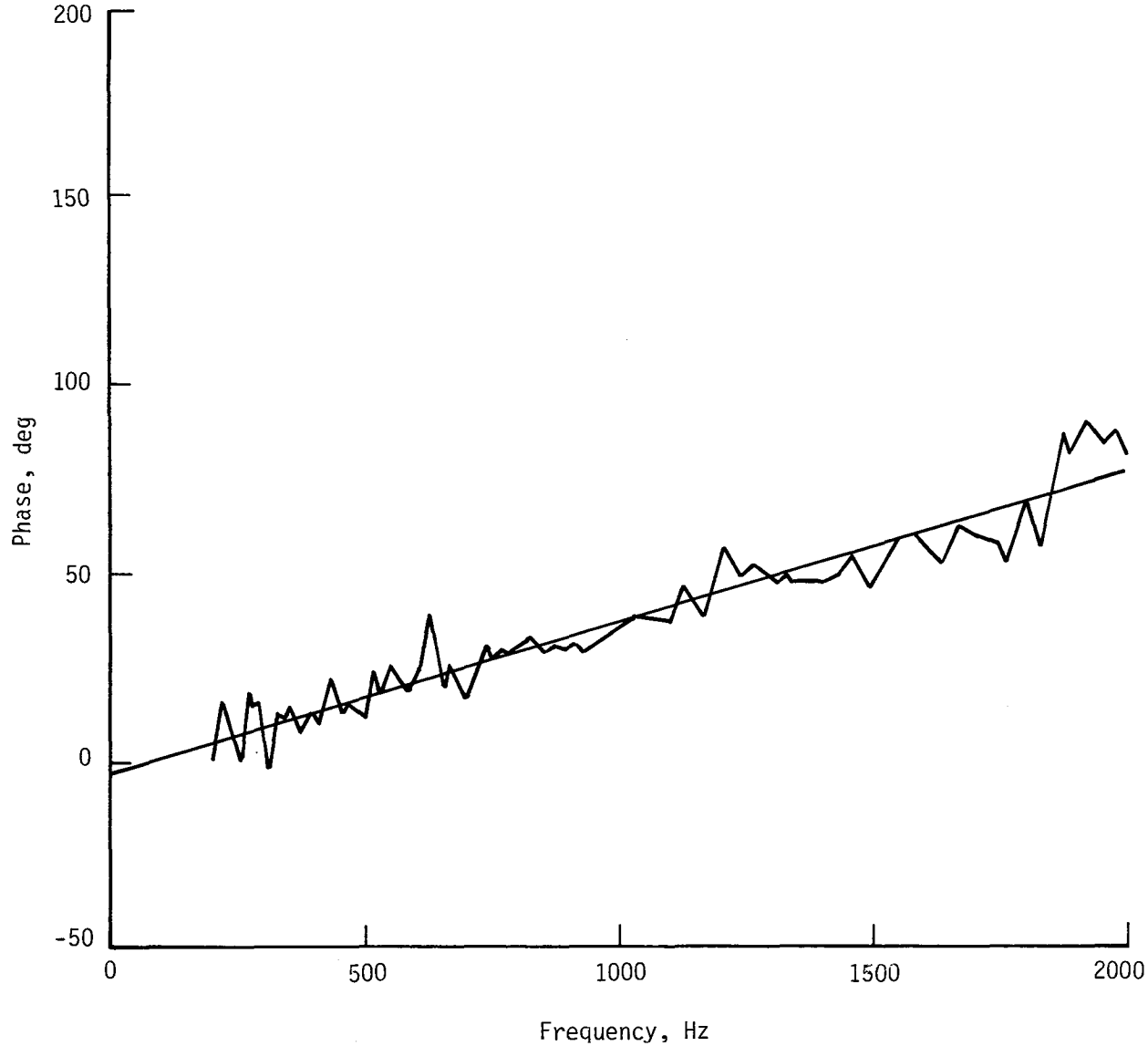

(a) Microphone pair B,A.

Figure 9.- Phase spectrum corresponding to soft-floor measurements of source position 1 for broadband measurements.

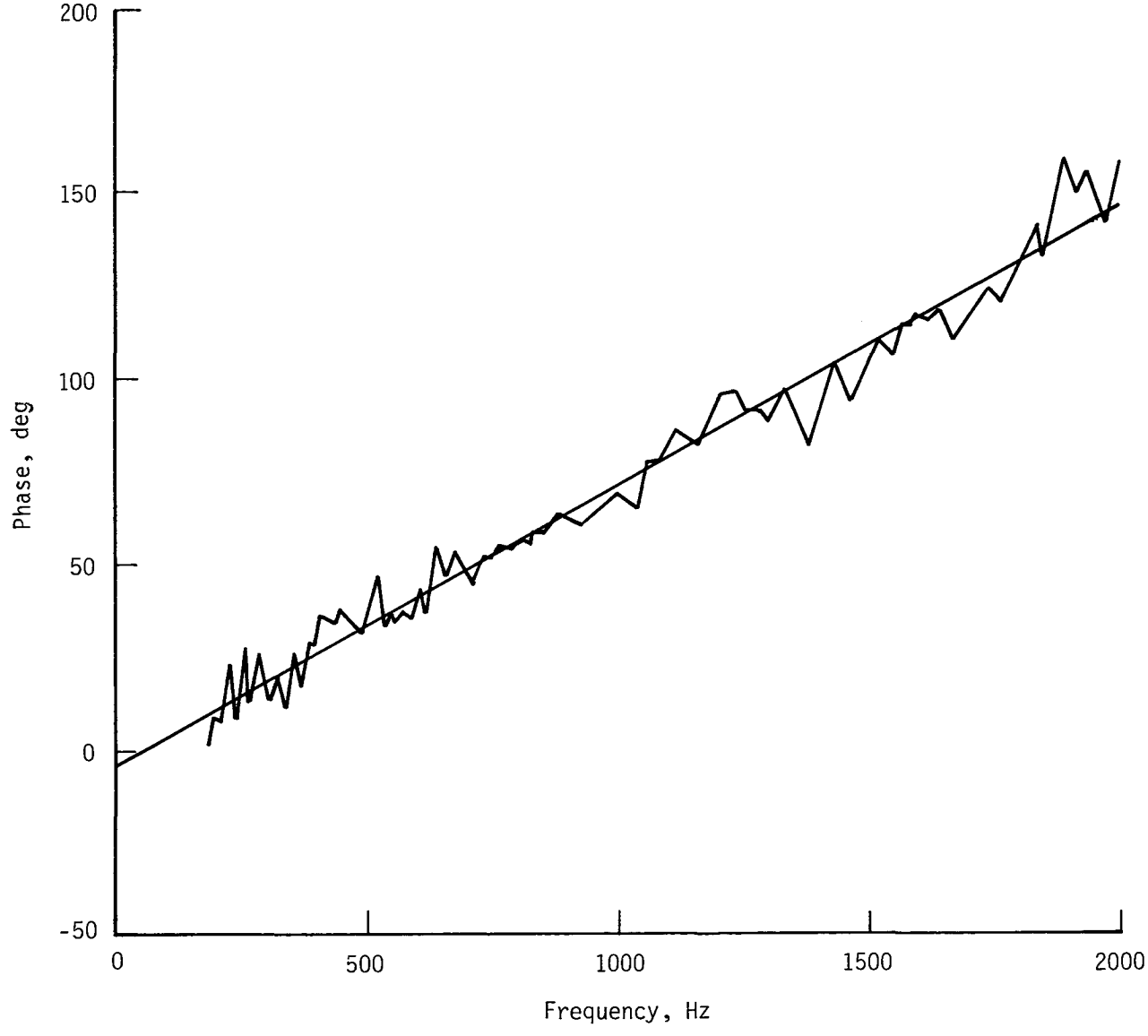

(b) Microphone pair B,C.

Figure 9.- Continued.

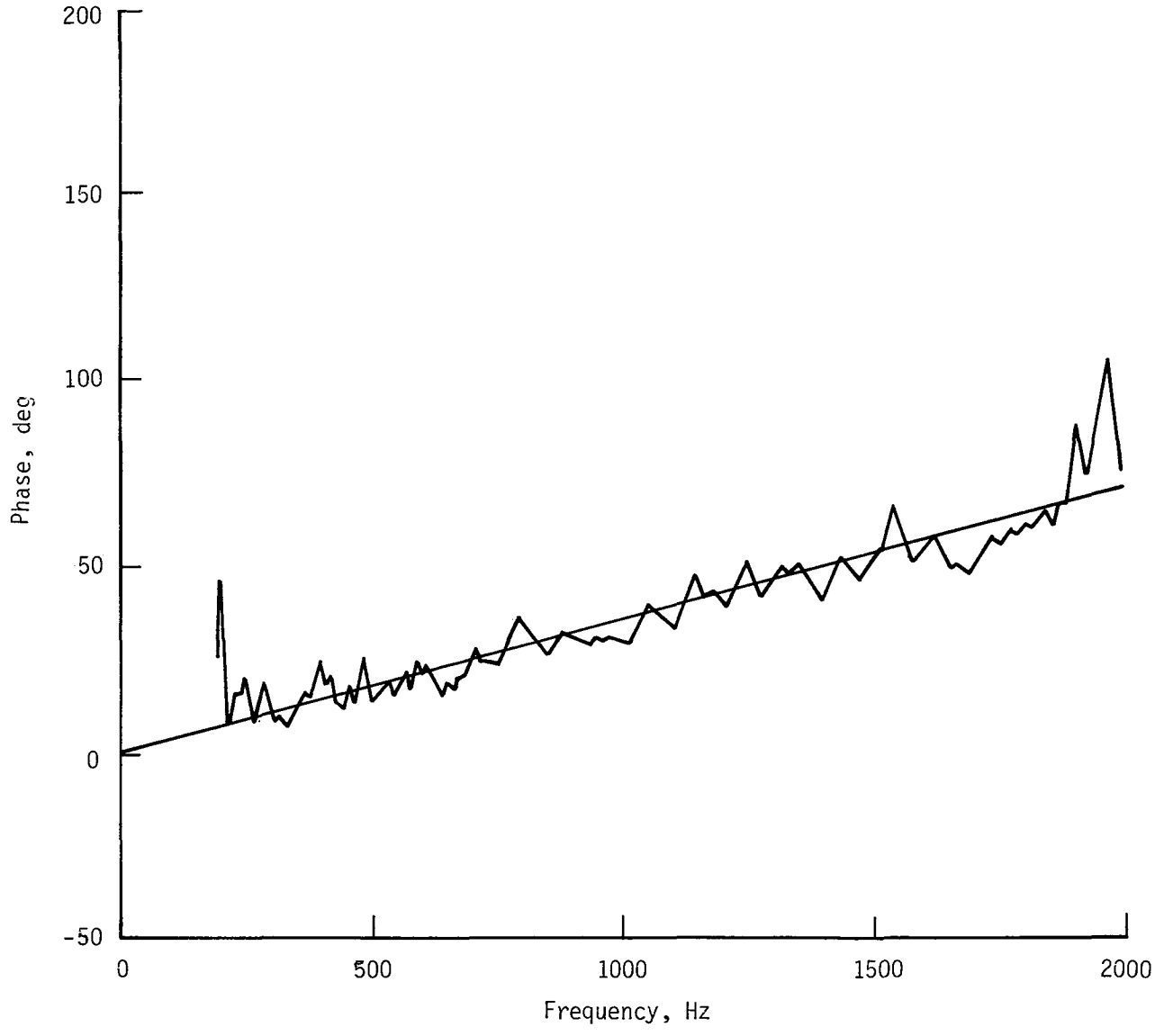

(c) Microphone pair E,D.

Figure 9.- Continued.

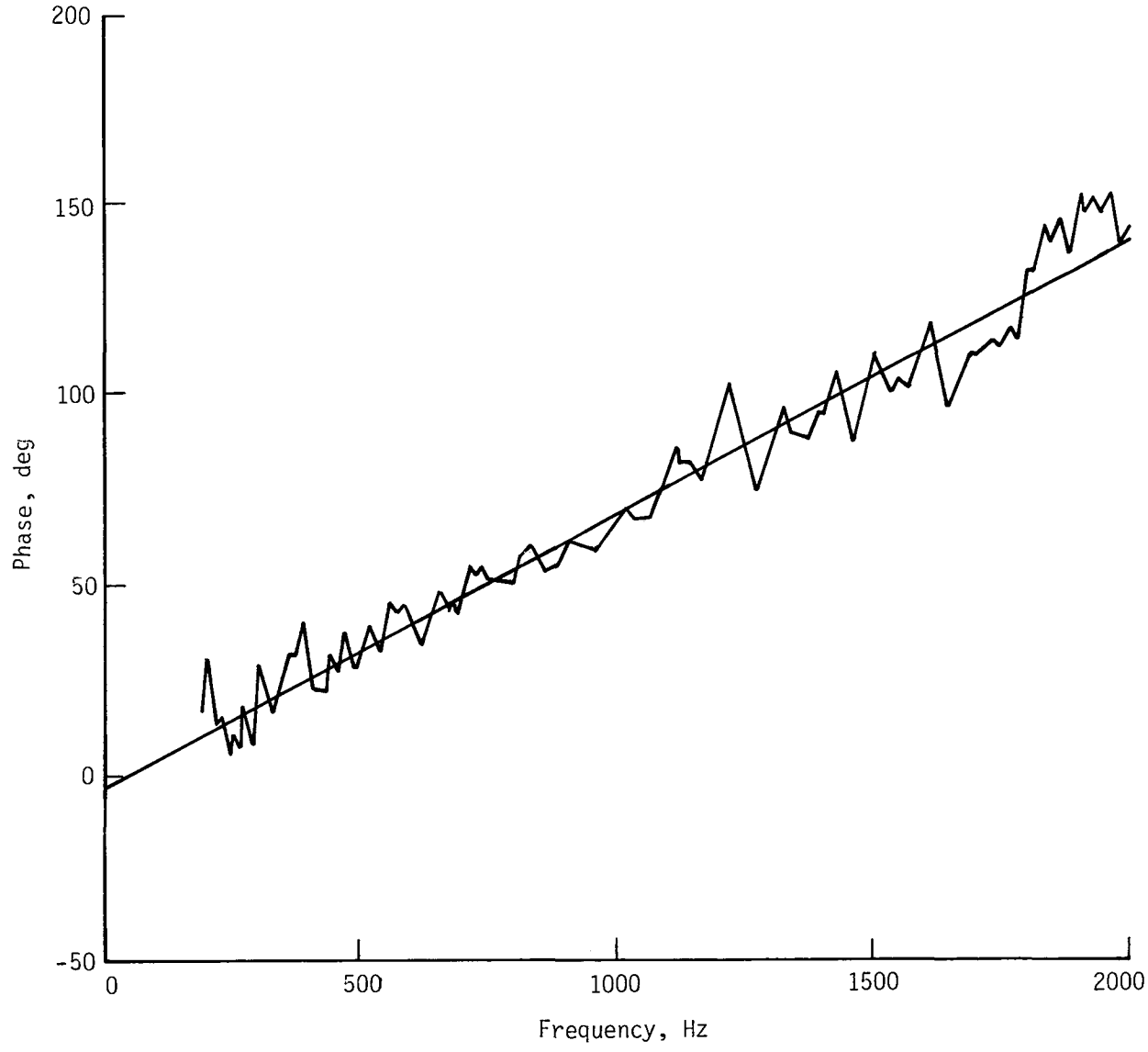

(d) Microphone pair E,F.

Figure 9.- Concluded.

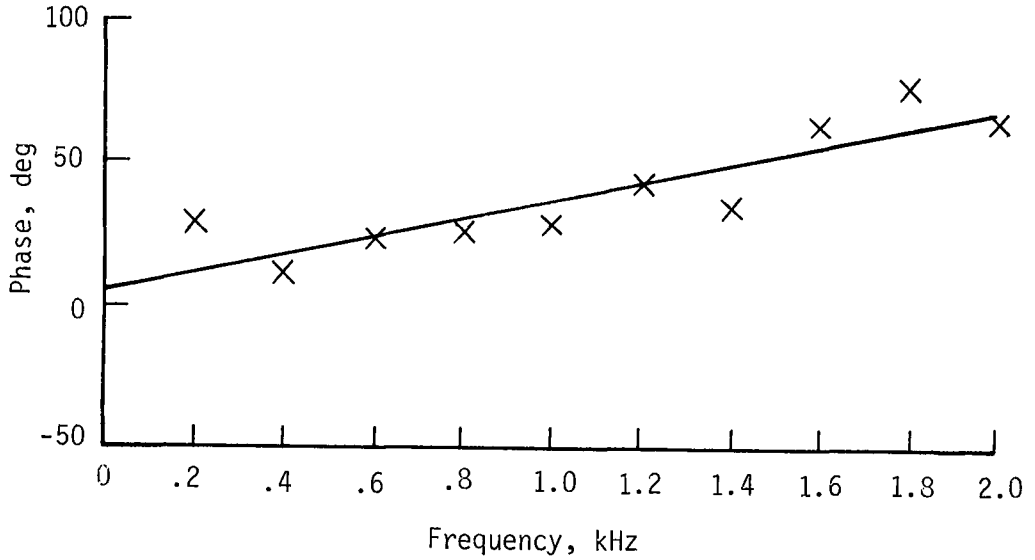

(a) Microphone pair B,A.

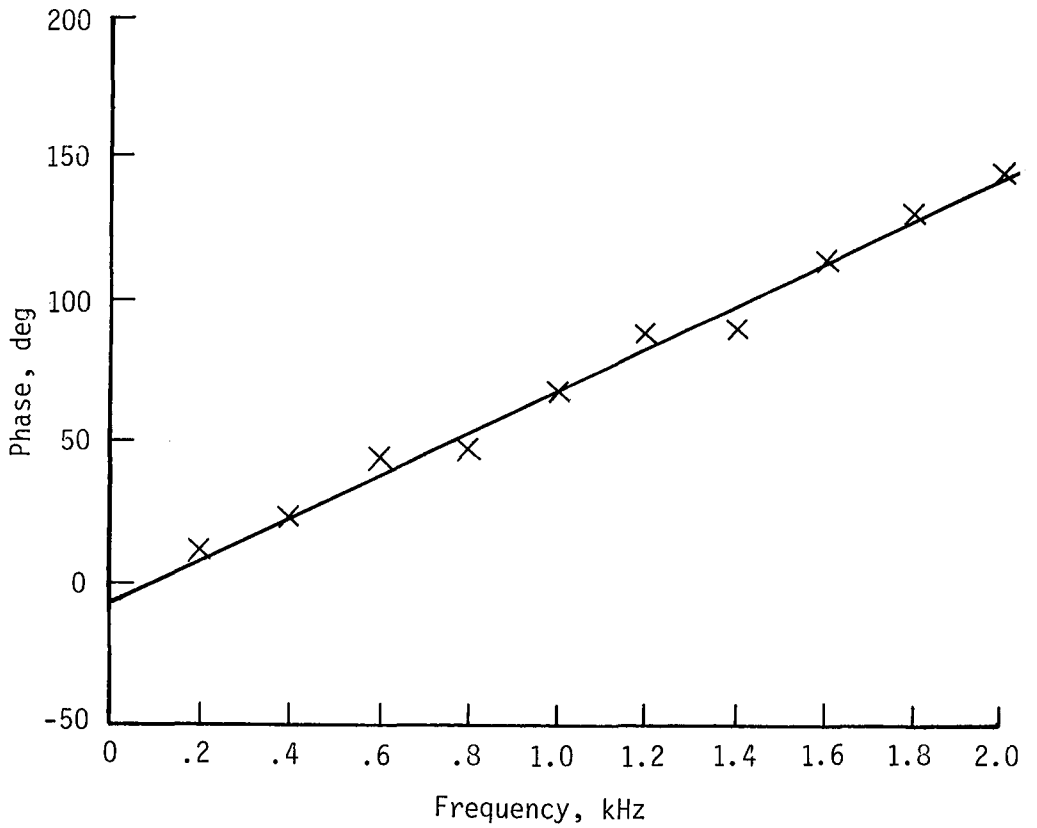

(b) Microphone pair B,C.

Figure 10.- Phase spectrum corresponding to hard-floor measurements of source position 1 for pure-tone measurements.

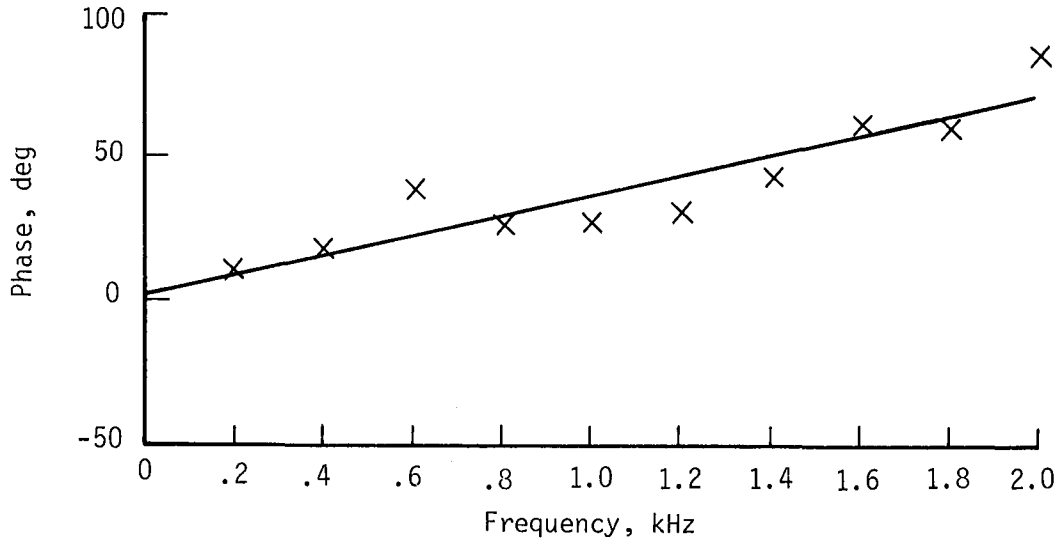

(c) Microphone pair E,D.

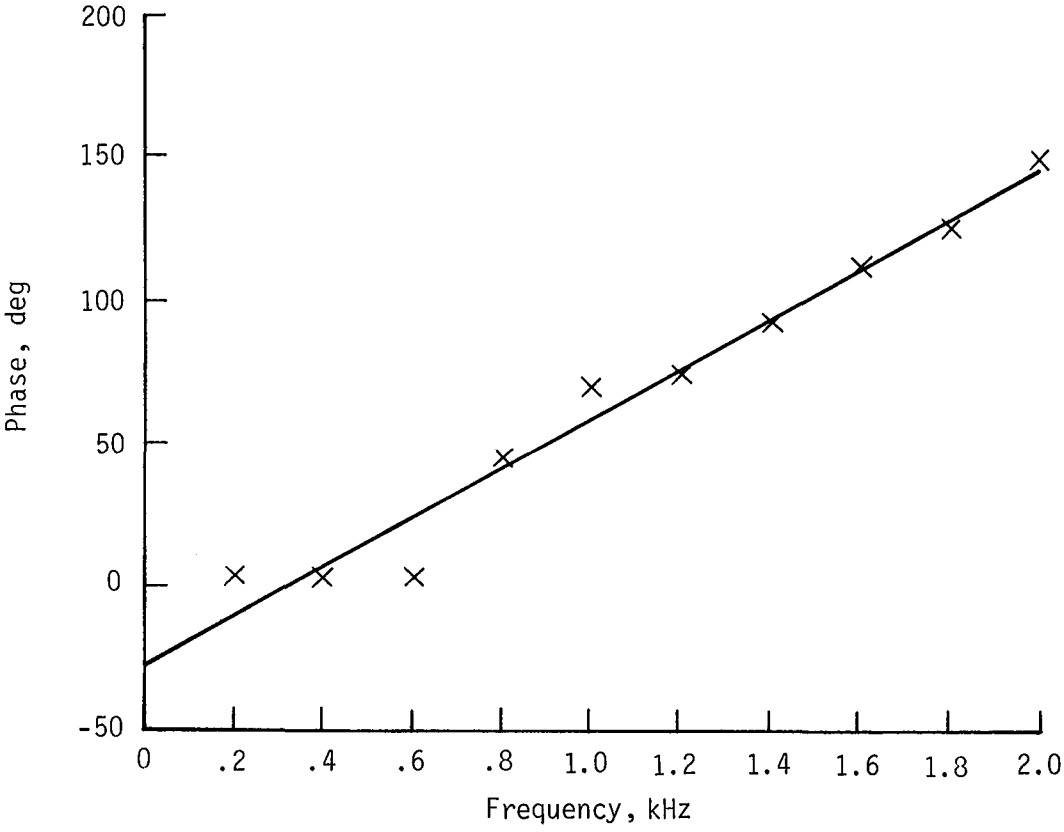

(d) Microphone pair E,F.

Figure 10.- Concluded.

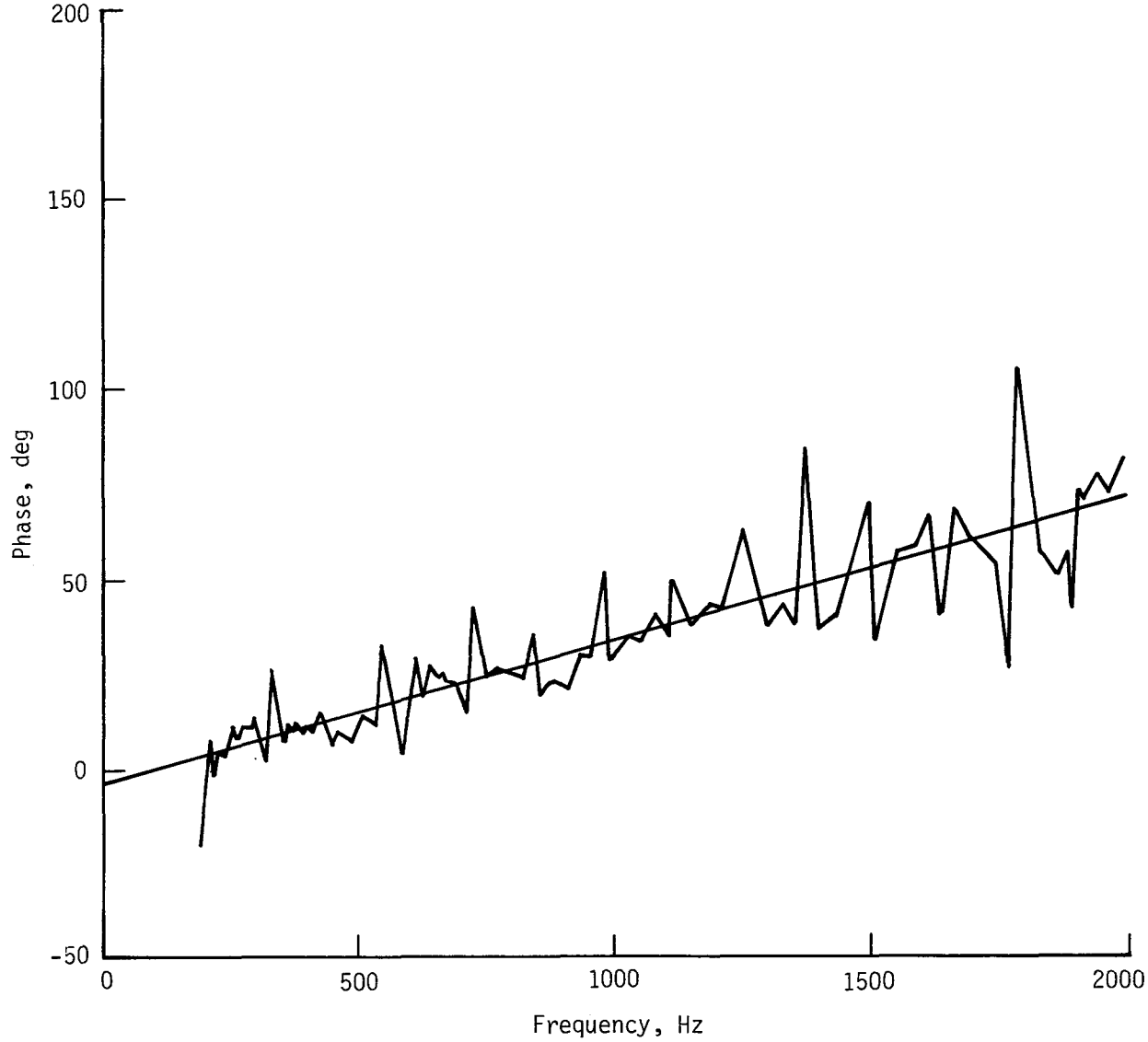

(a) Microphone pair B,A.

Figure 11.- Phase spectrum corresponding to hard-floor measurements of source position 1 for broadband measurements.

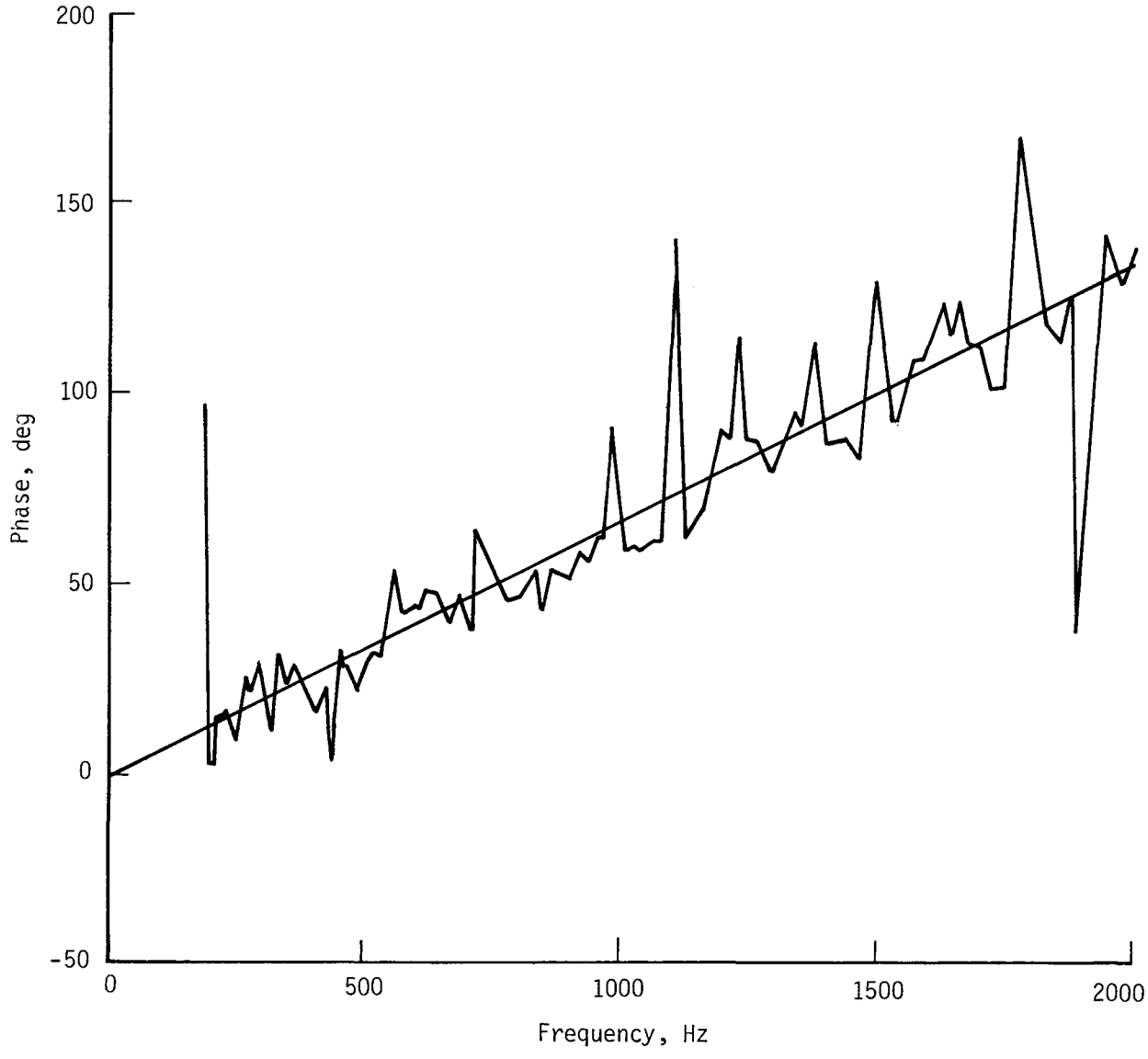

(b) Microphone pair B,C.

Figure 11.- Continued.

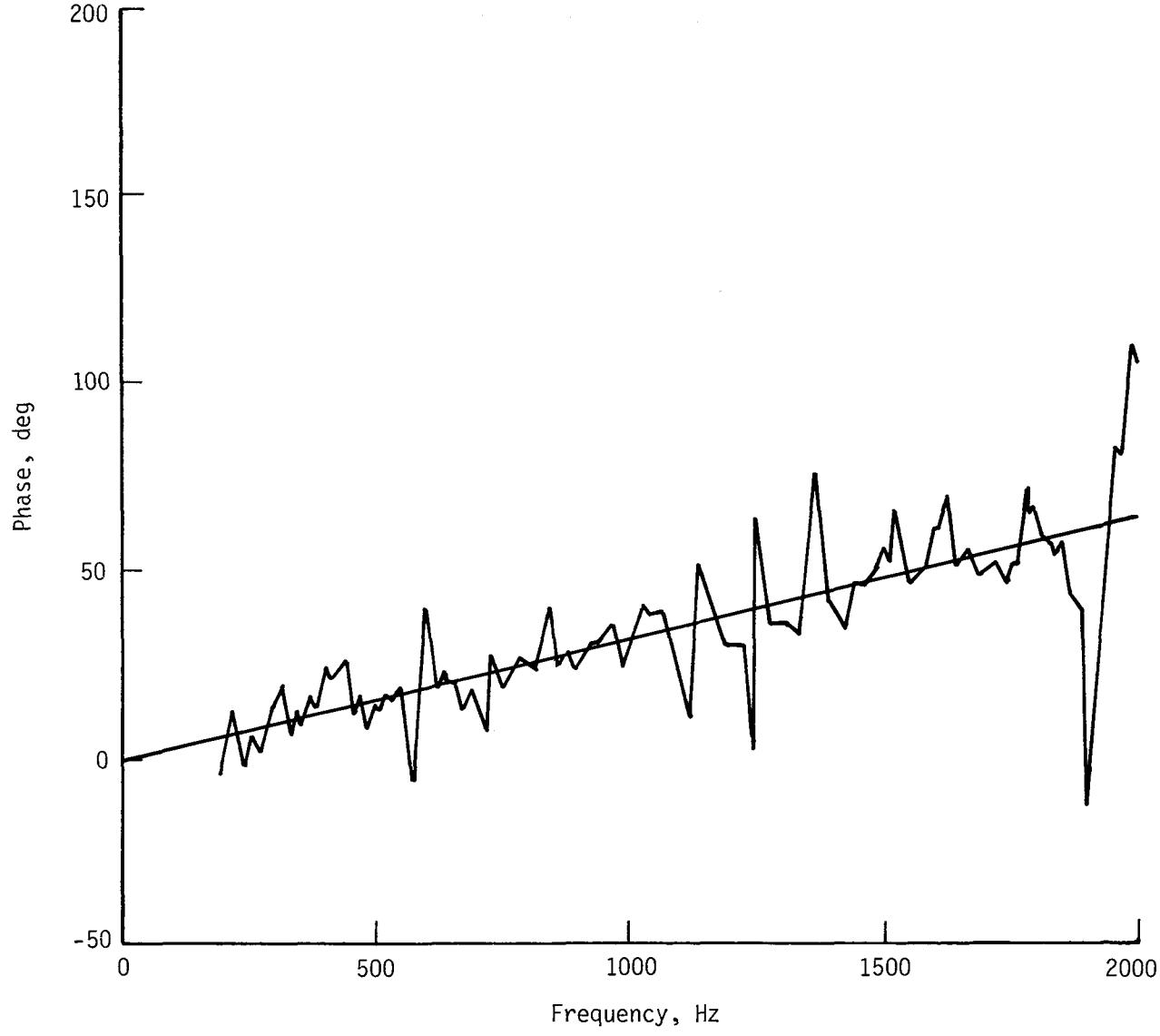

(c) Microphone pair E,D.

Figure 11.- Continued.

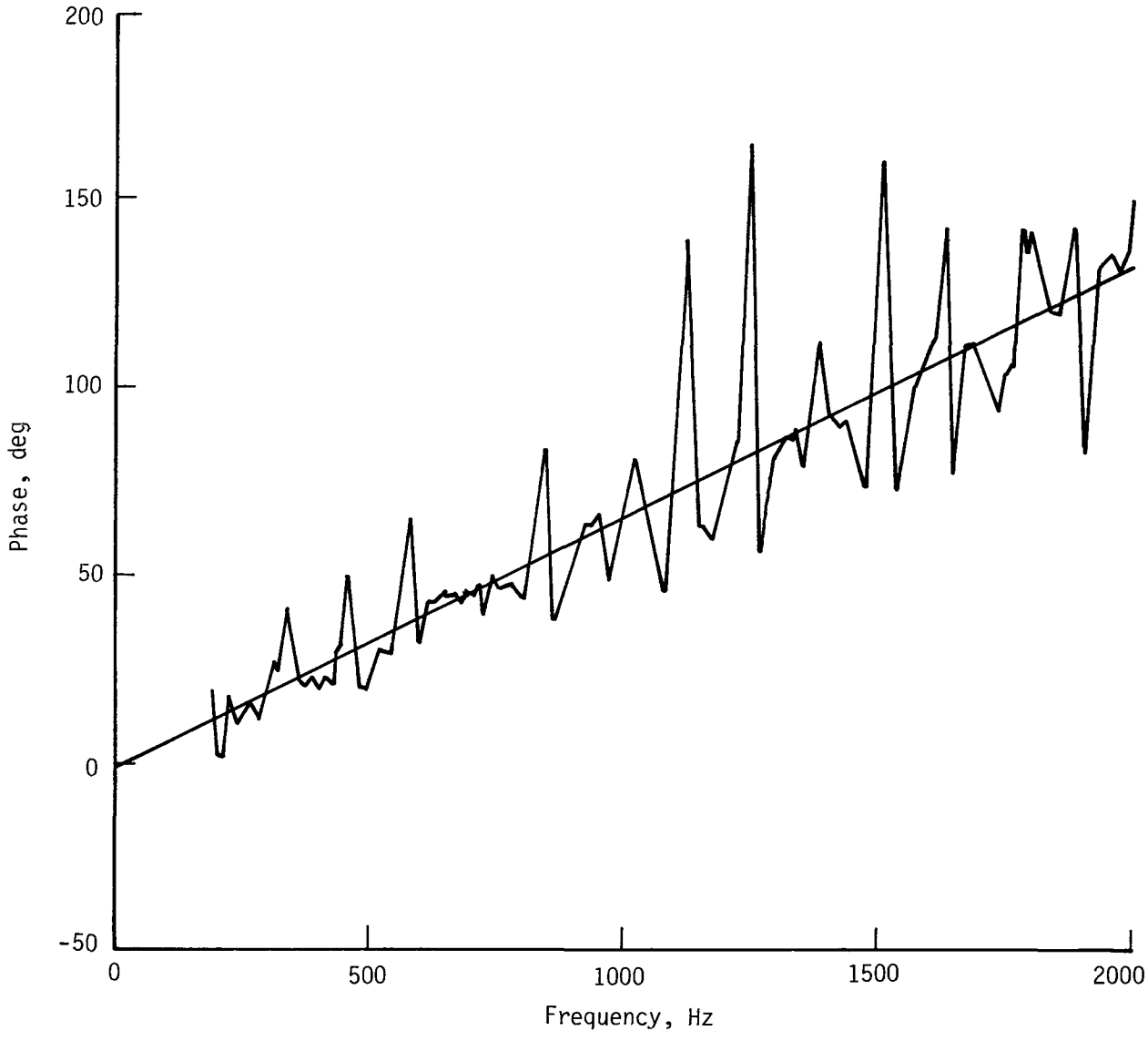

(d) Microphone pair E,F.

Figure 11.- Concluded.

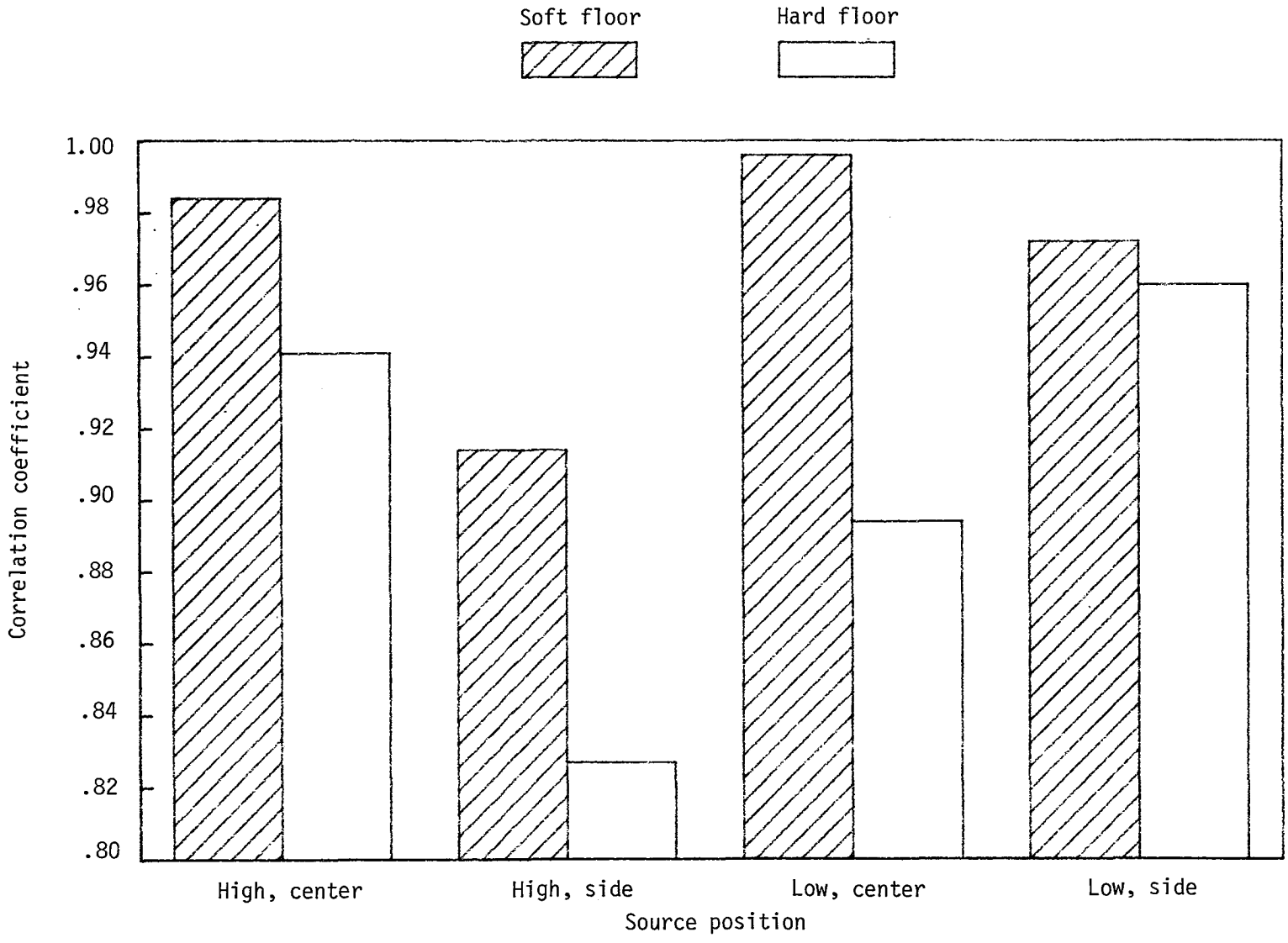

Figure 12.- Phase-frequency correlation of pure-tone data.

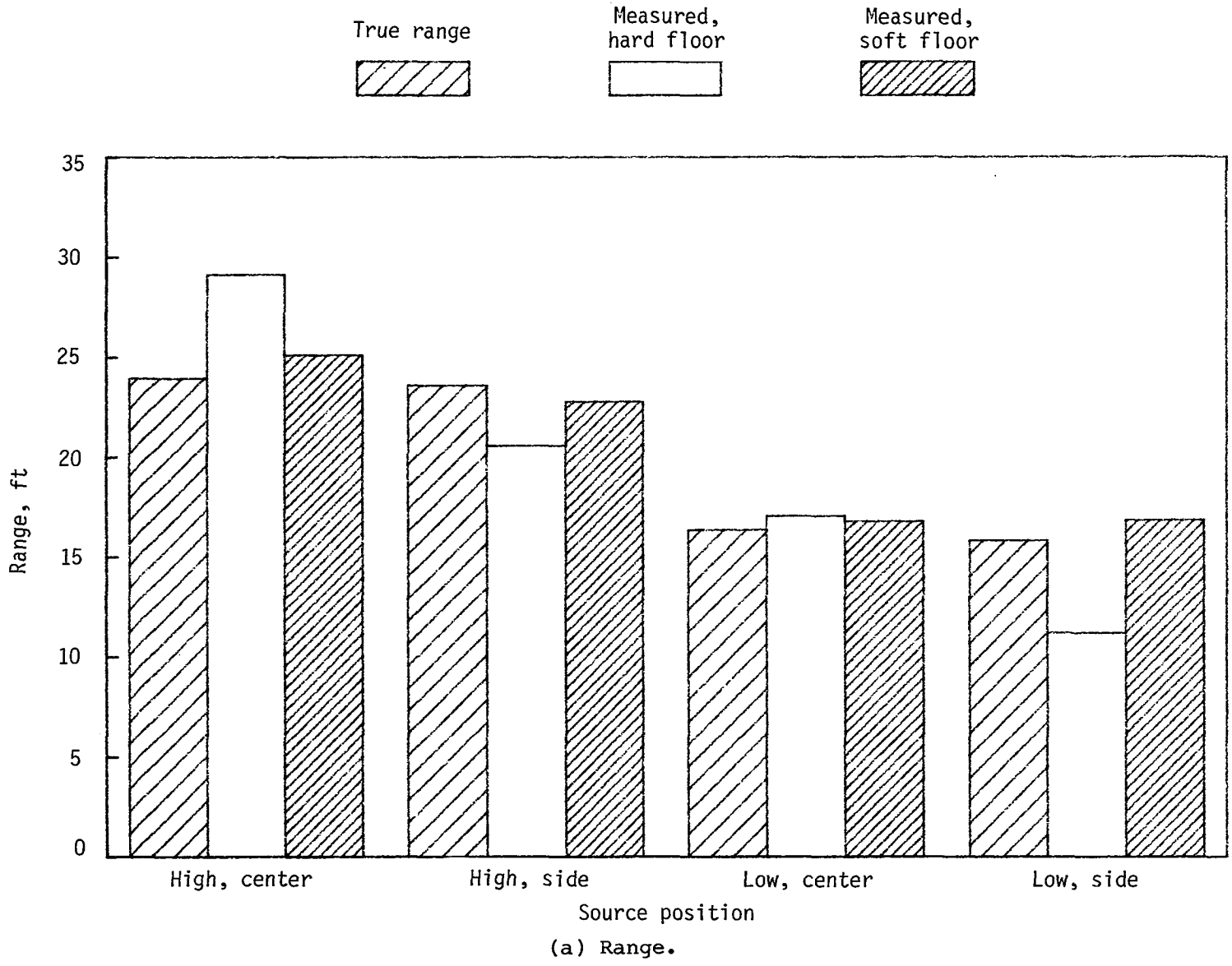

(a) Range.

Figure 13.- Comparison of hard-floor and soft-floor measurements for array I obtained from pure-tone data and by theodolite.

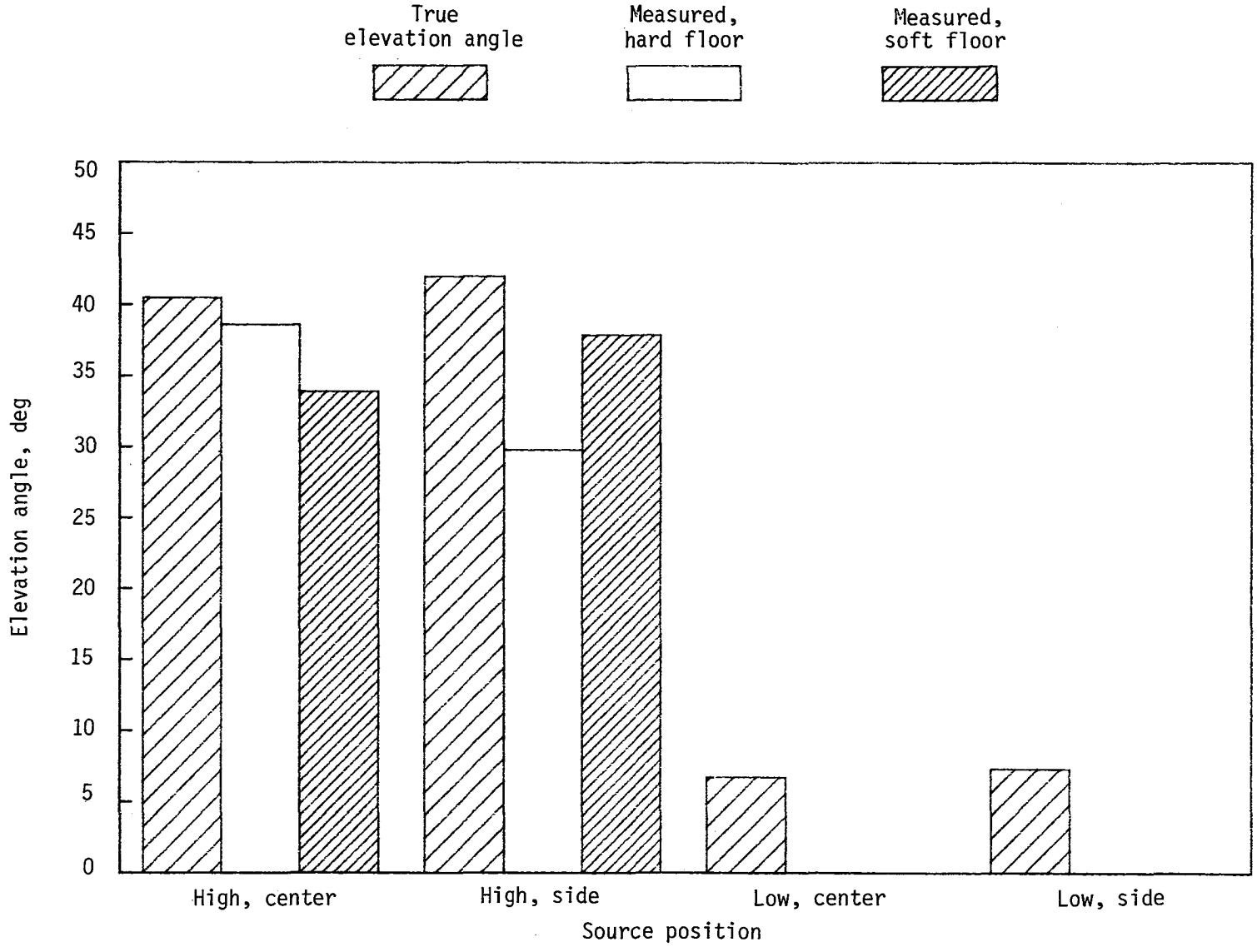

(b) Elevation angle. Measured elevation angles for low source positions are 0° for hard and soft floors.

Figure 13.- Continued.

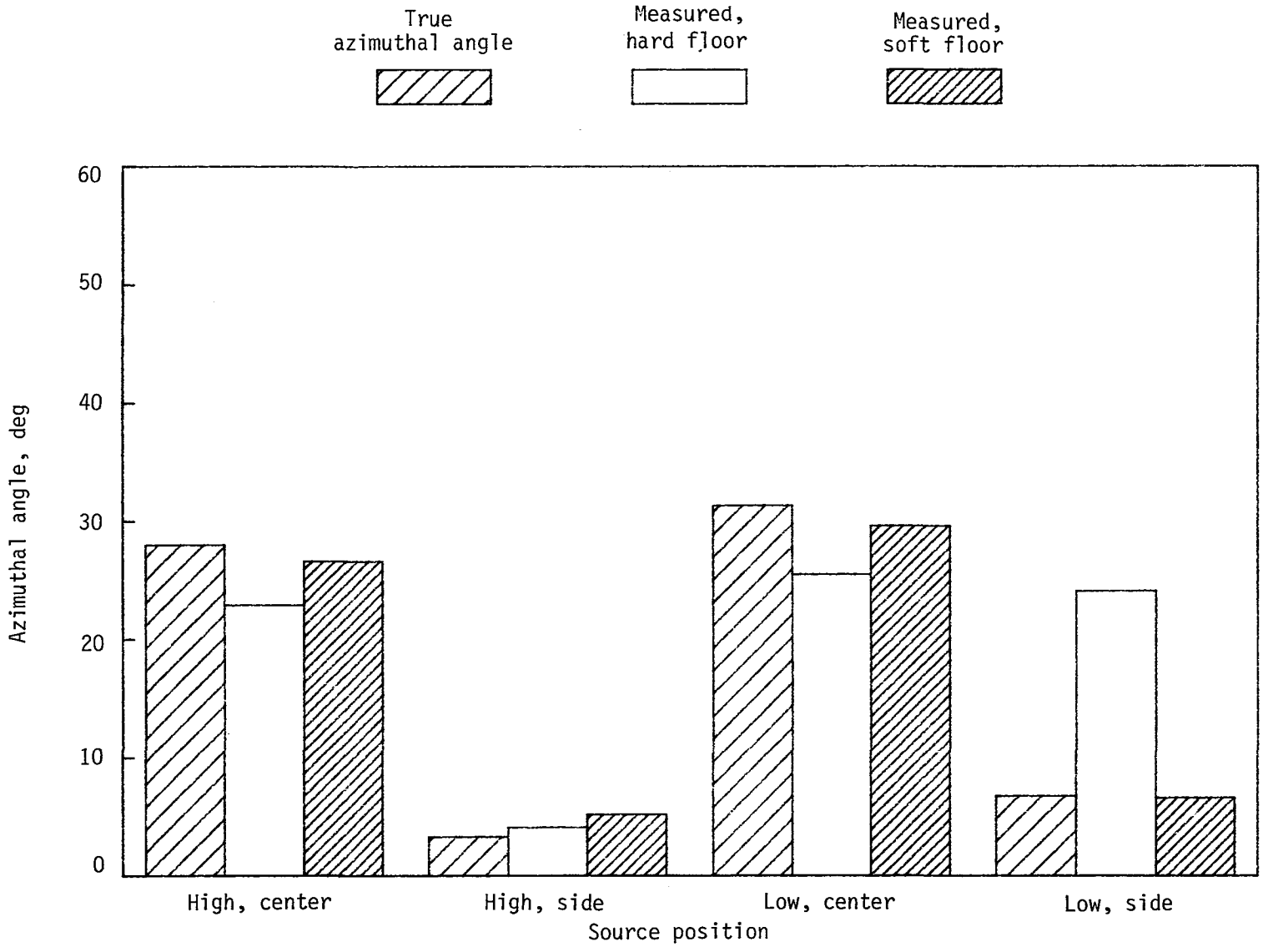

(c) Azimuthal angle.

Figure 13.- Concluded.

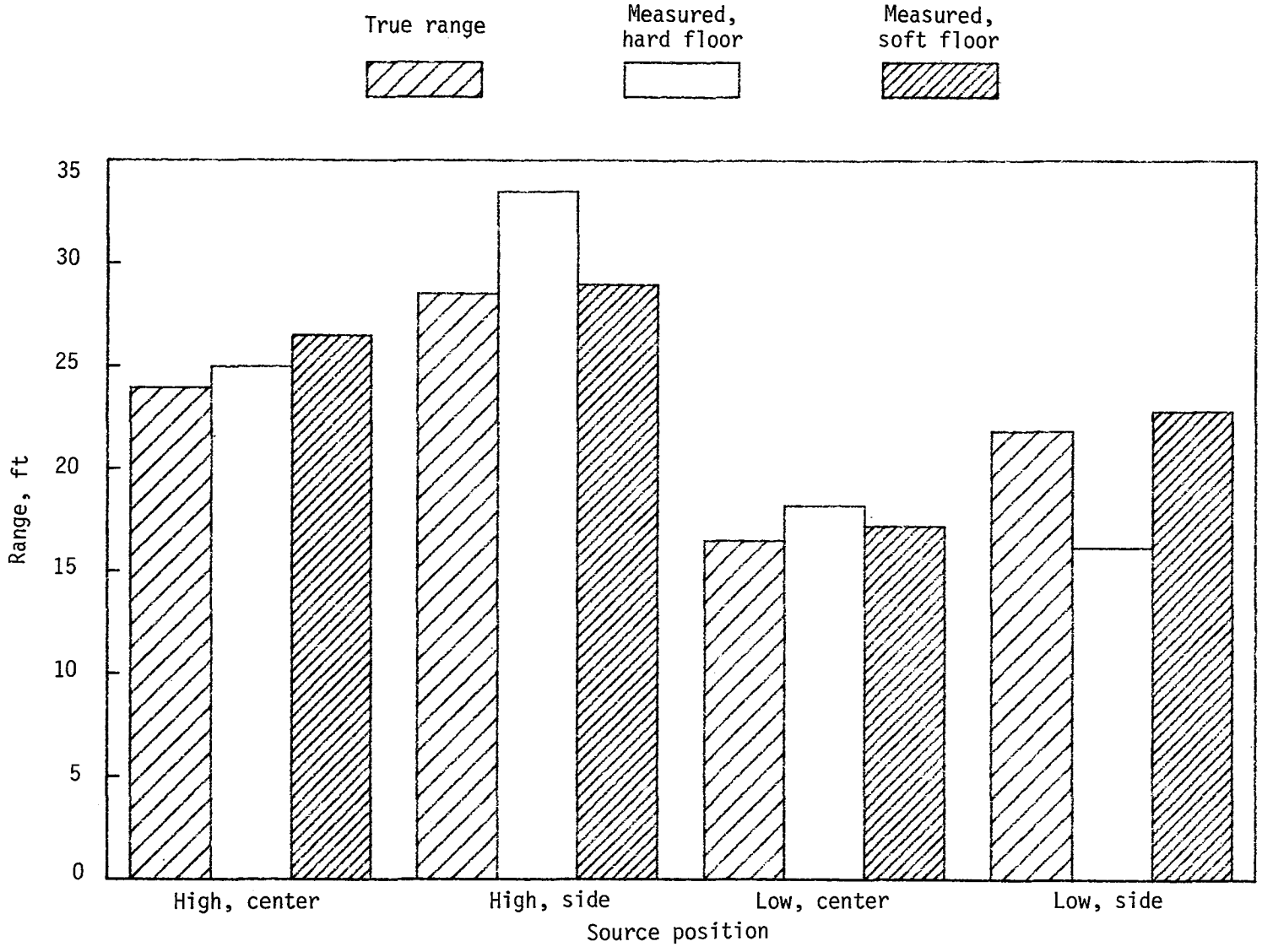

(a) Range.

Figure 14.- Comparison of hard-floor and soft-floor measurements for array II obtained from pure-tone data and by theodolite.

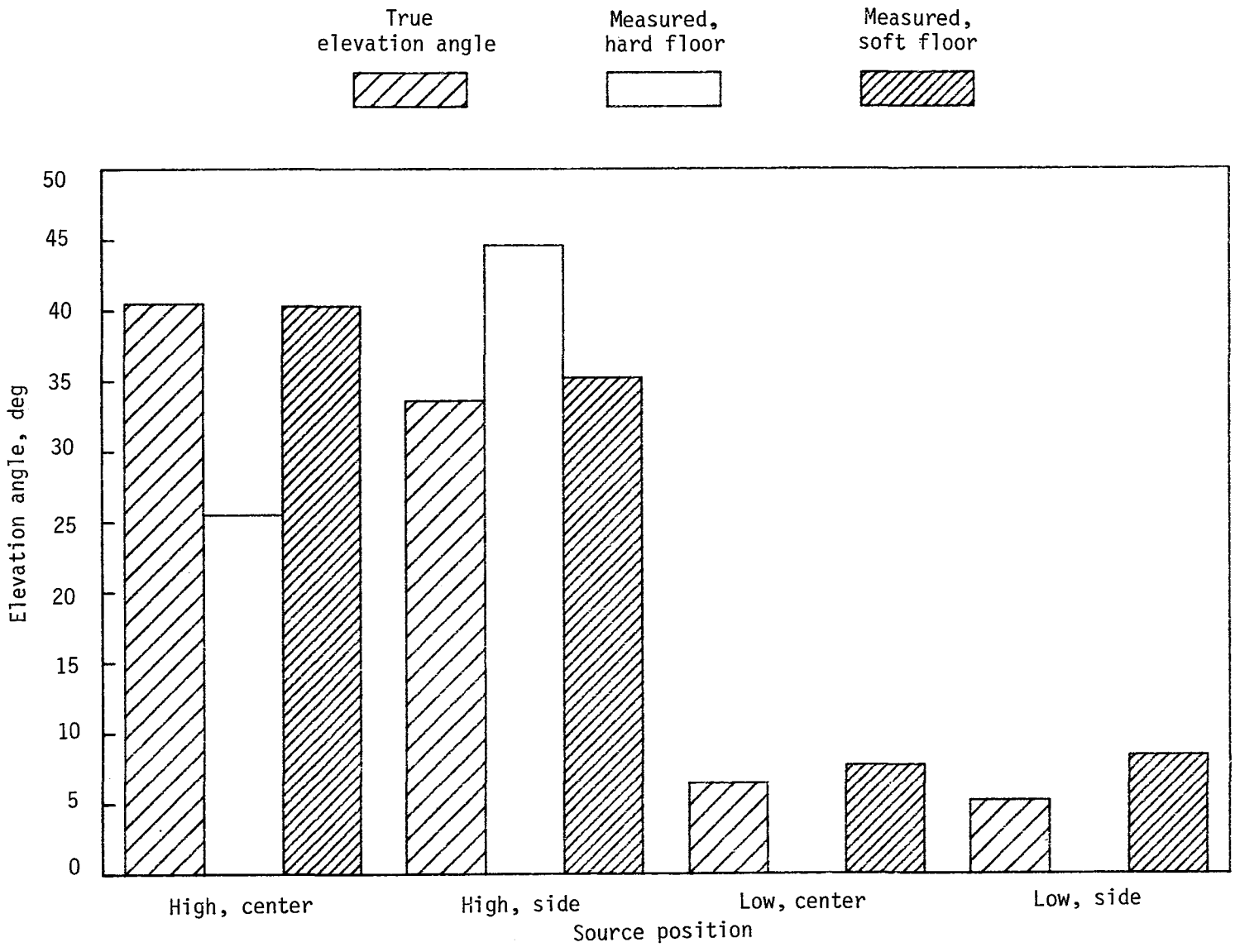

(b) Elevation angle. Measured elevation angles for low source positions are 0° for hard floor.

Figure 14.- Continued.

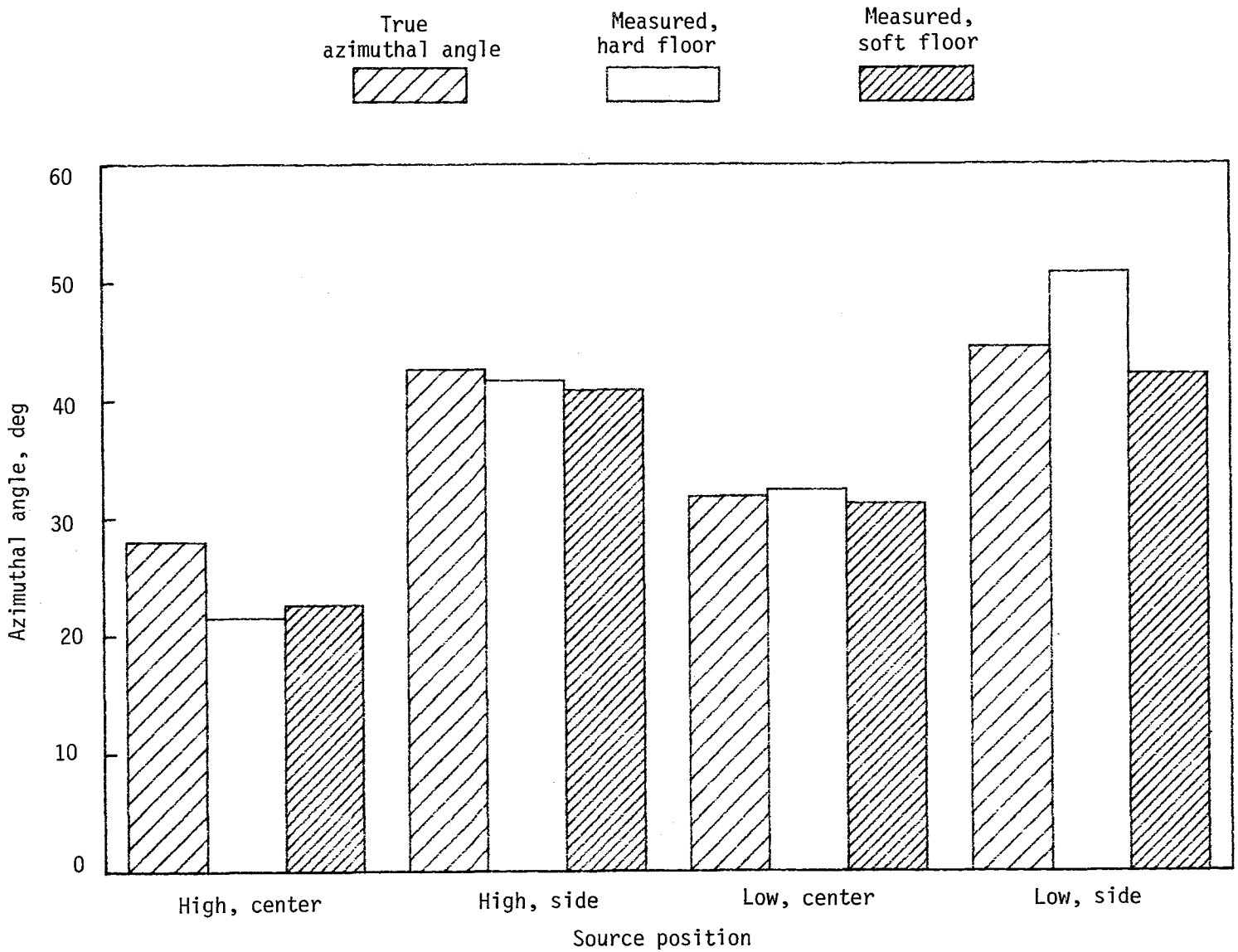

(c) Azimuthal angle.

Figure 14.- Concluded.

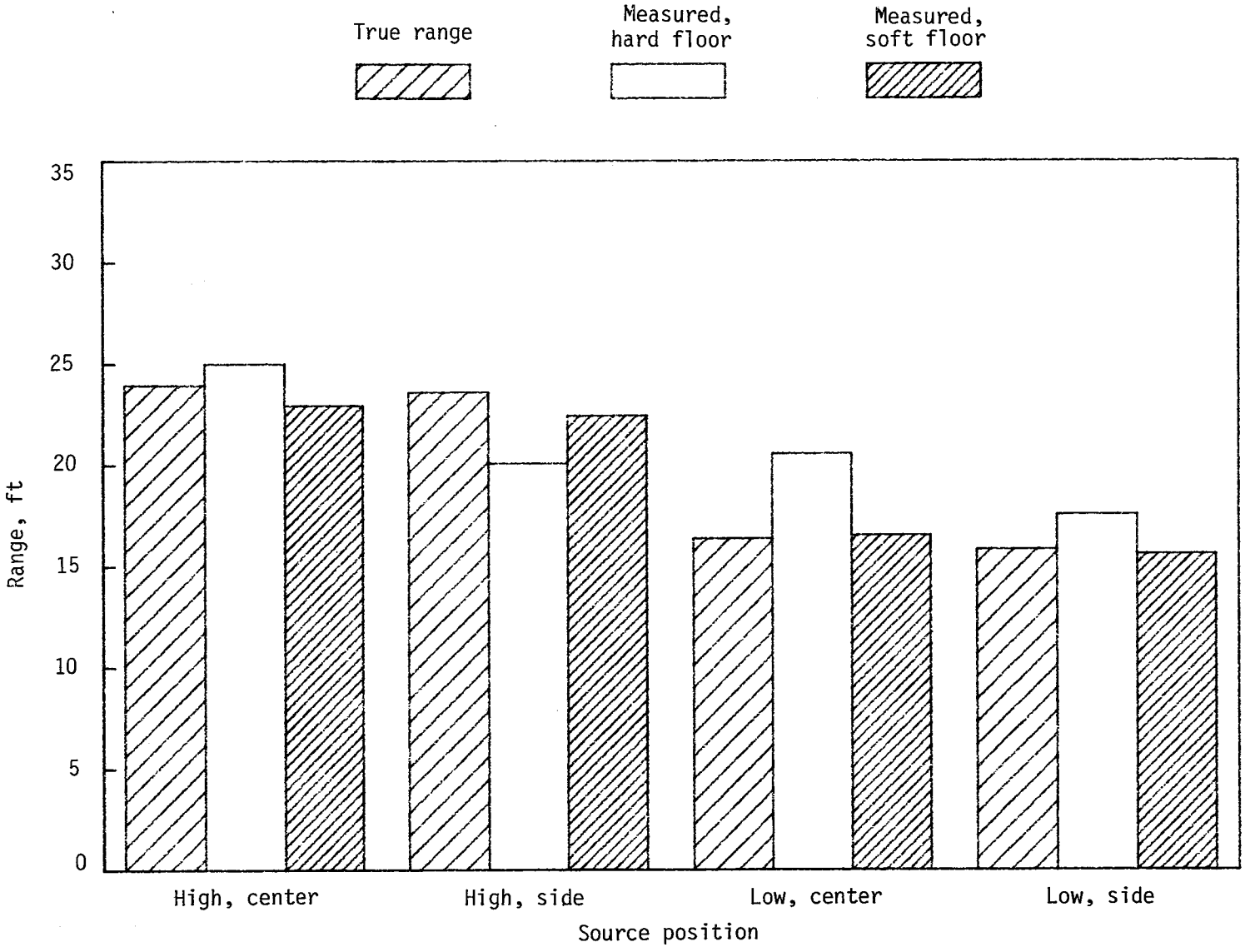

(a) Range.

Figure 15.- Comparison of hard-floor and soft-floor measurements for array I obtained from broadband data and by theodolite.

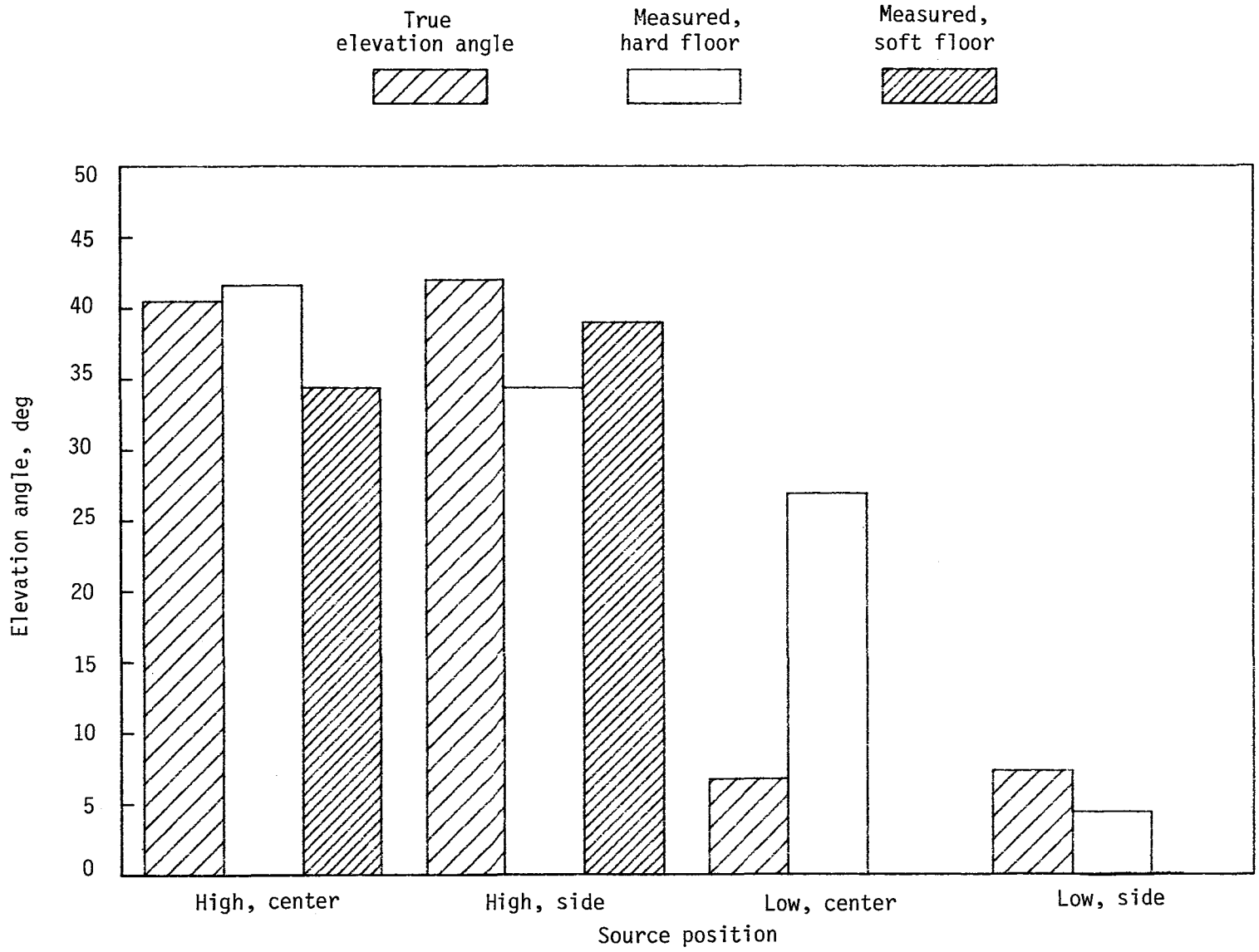

(b) Elevation angle. Measured elevation angles for low source positions are 0° for soft floor.

Figure 15.- Continued.

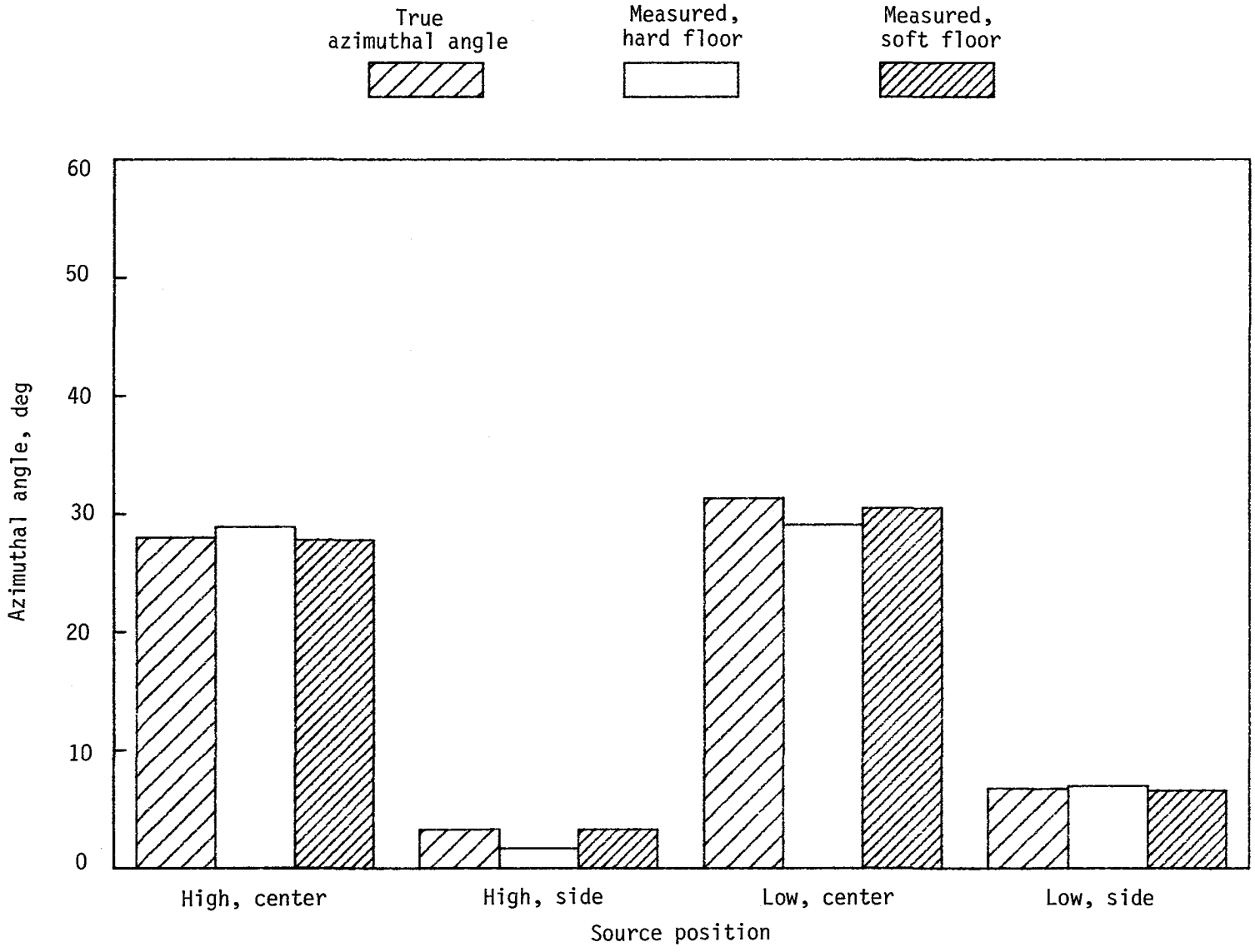

(c) Azimuthal angle.

Figure 15.- Concluded.

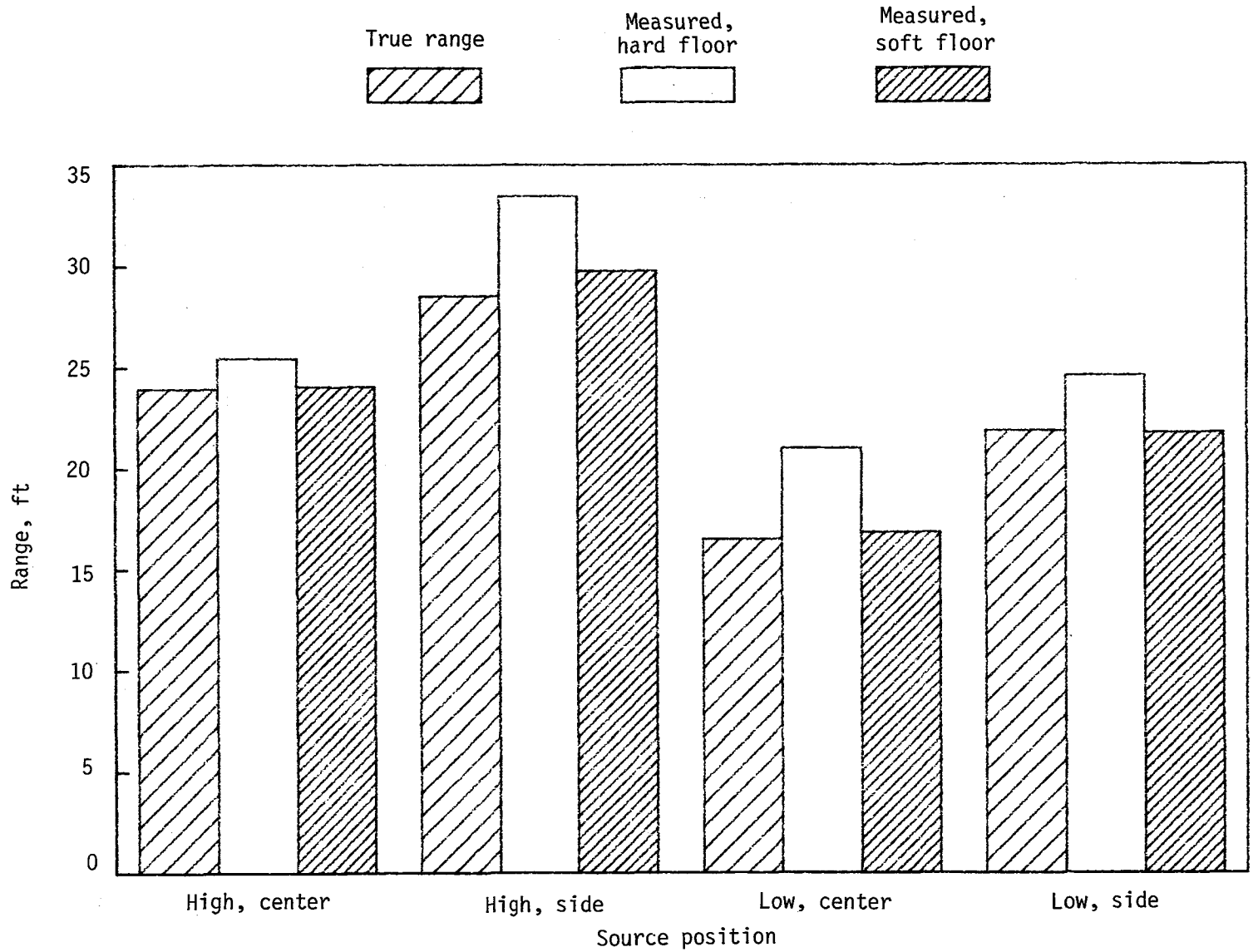

(a) Range.

Figure 16.- Comparison of hard-floor and soft-floor measurements for array II obtained from broadband data and by theodolite.

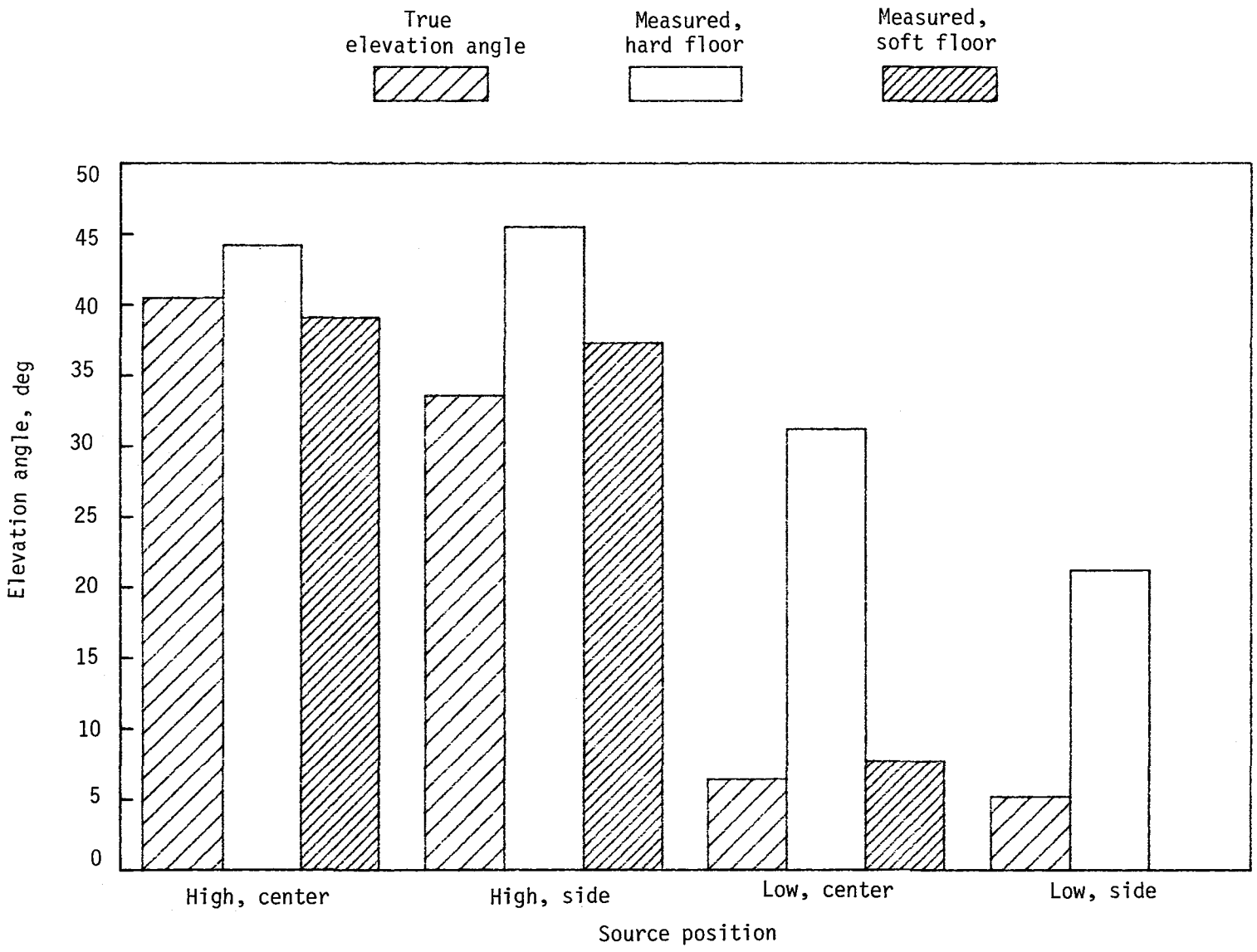

(b) Elevation angle. Measured elevation angle for low, side source position is 0° for soft floor.

Figure 16.- Continued.

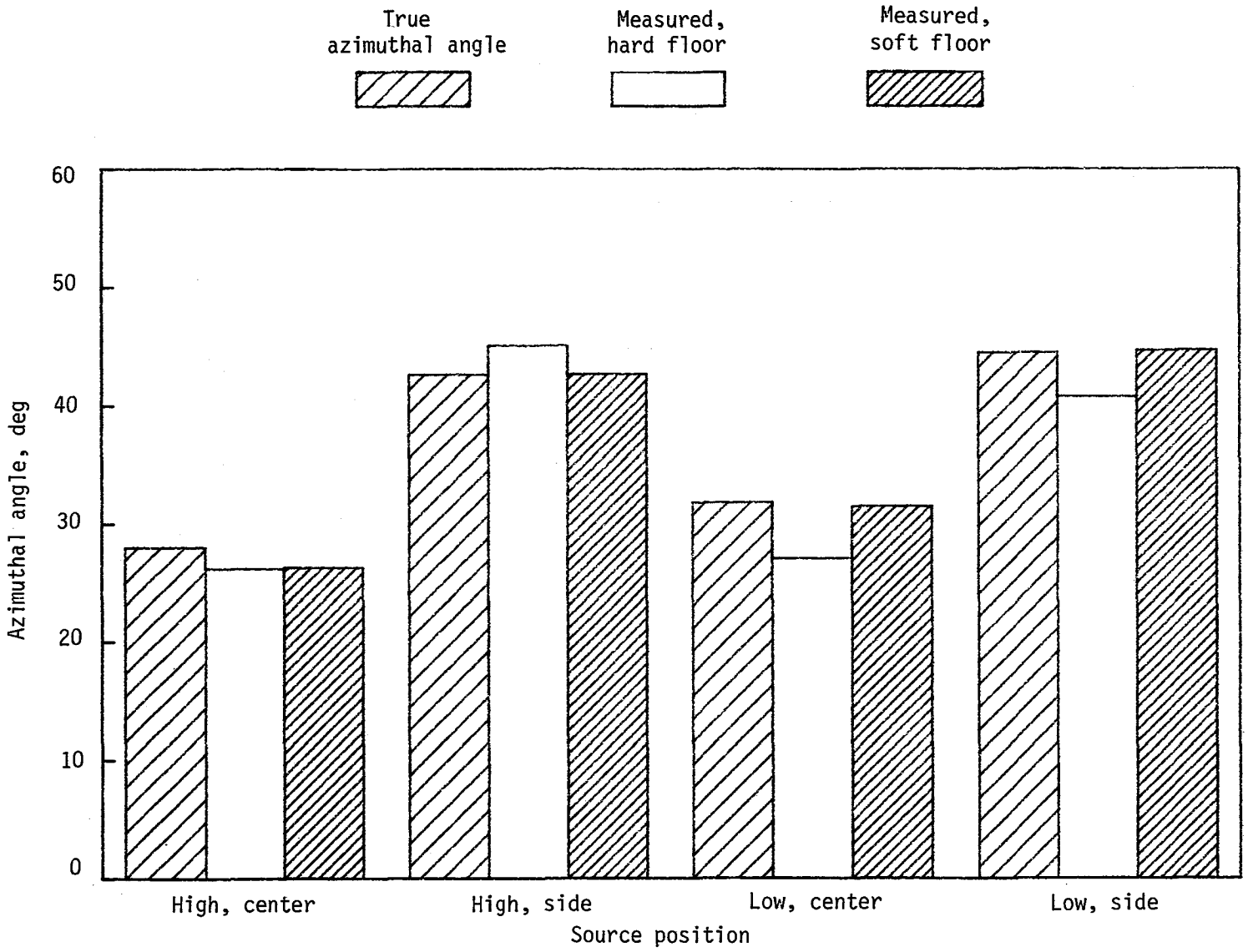

(c) Azimuthal angle.

Figure 16.- Concluded.

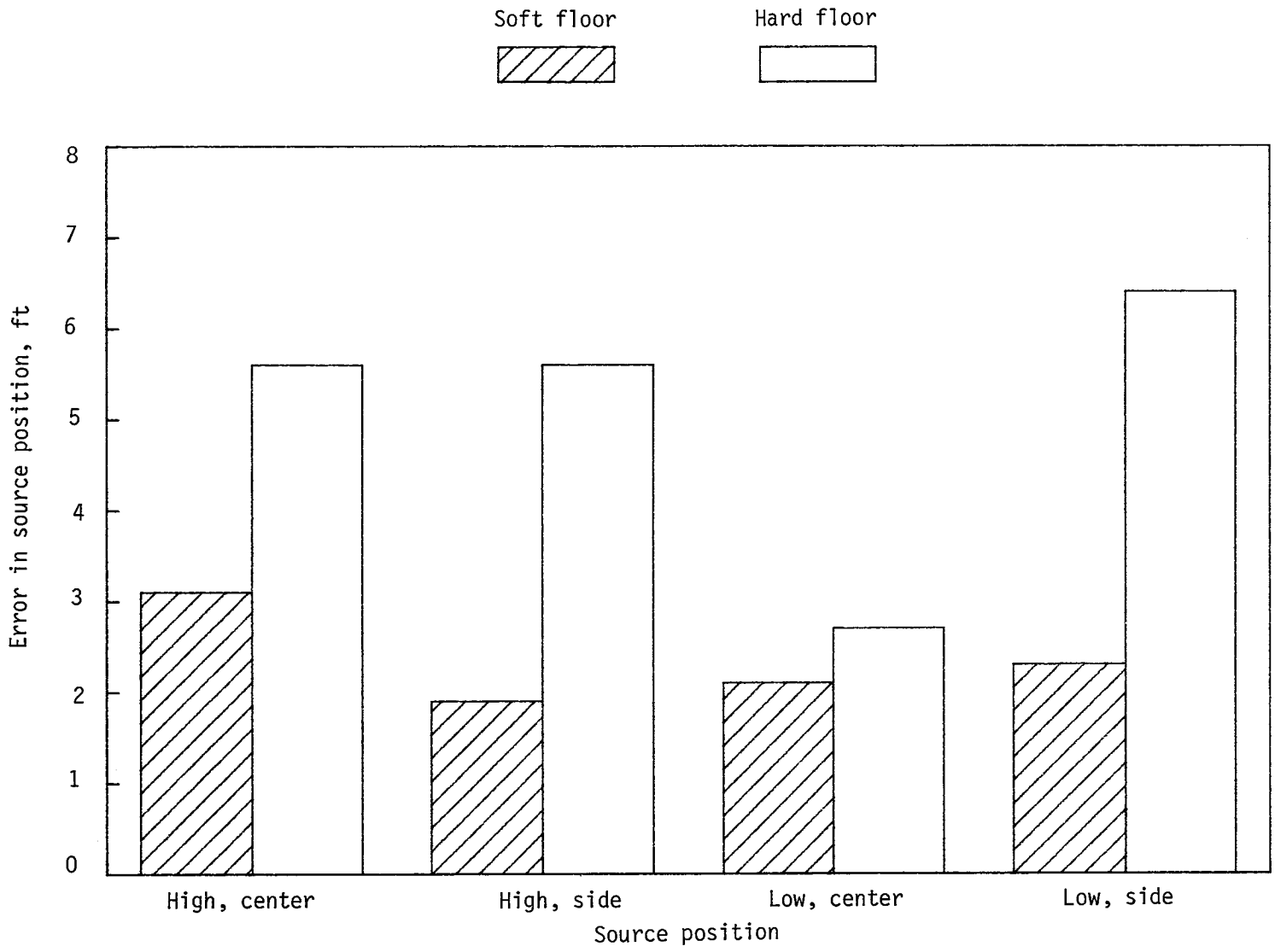

(a) Pure-tone data.

Figure 17.- Comparison of source positions measured from acoustic data with those obtained by theodolite.

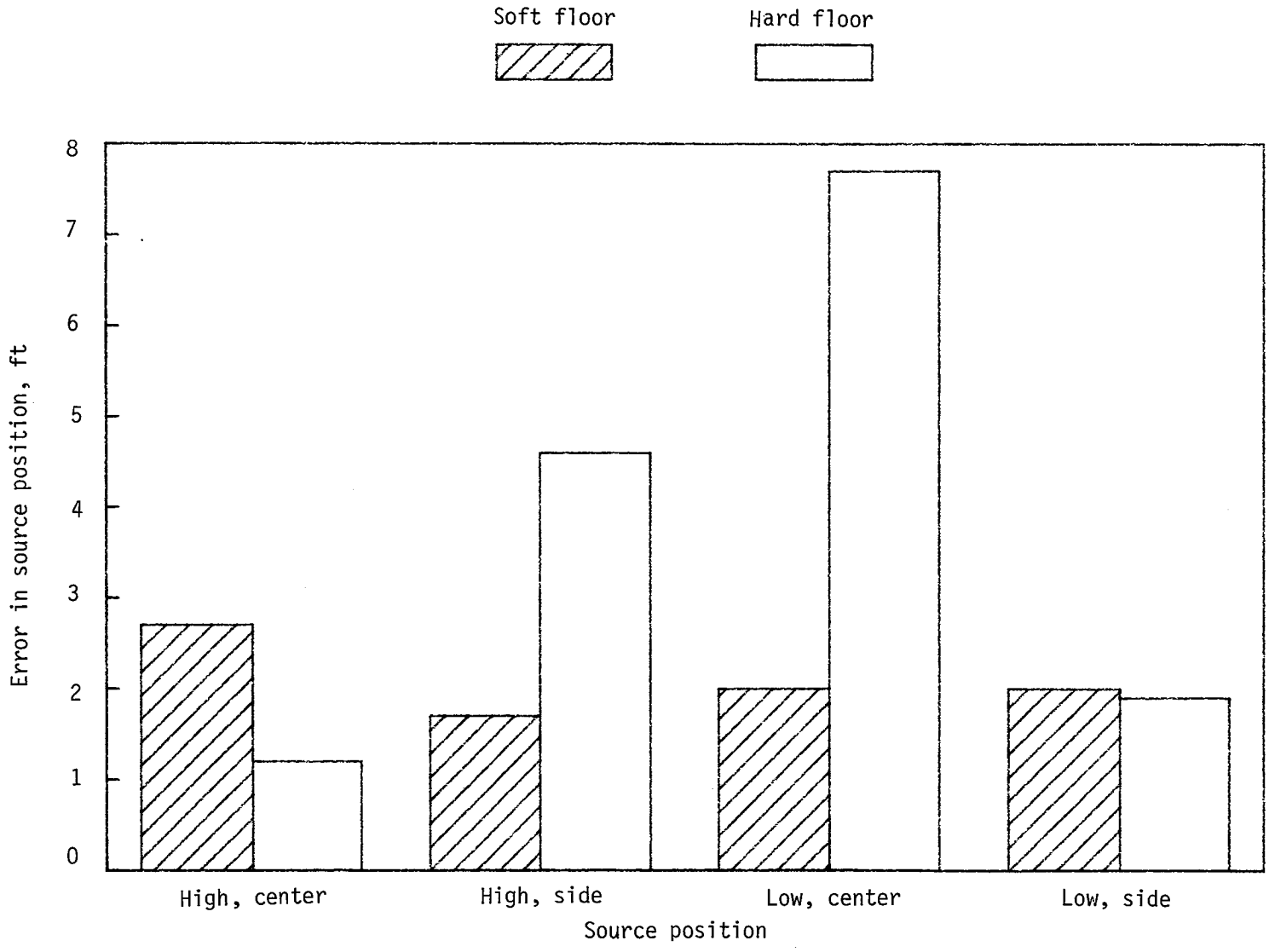

(b) Broadband data.

Figure 17.- Concluded.

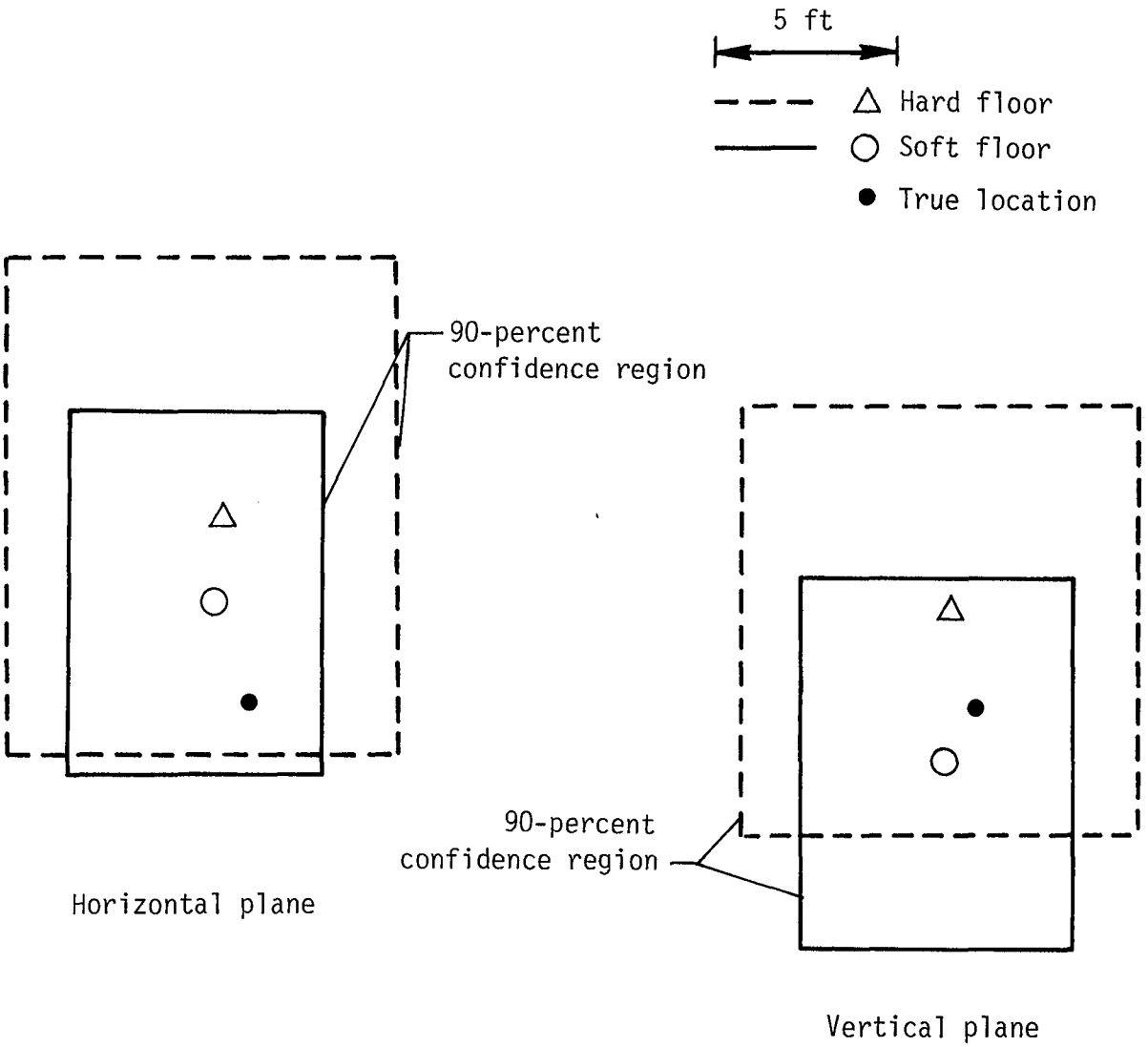

(a) Source position 1.

Figure 18.- Location accuracy and precision for four source positions.

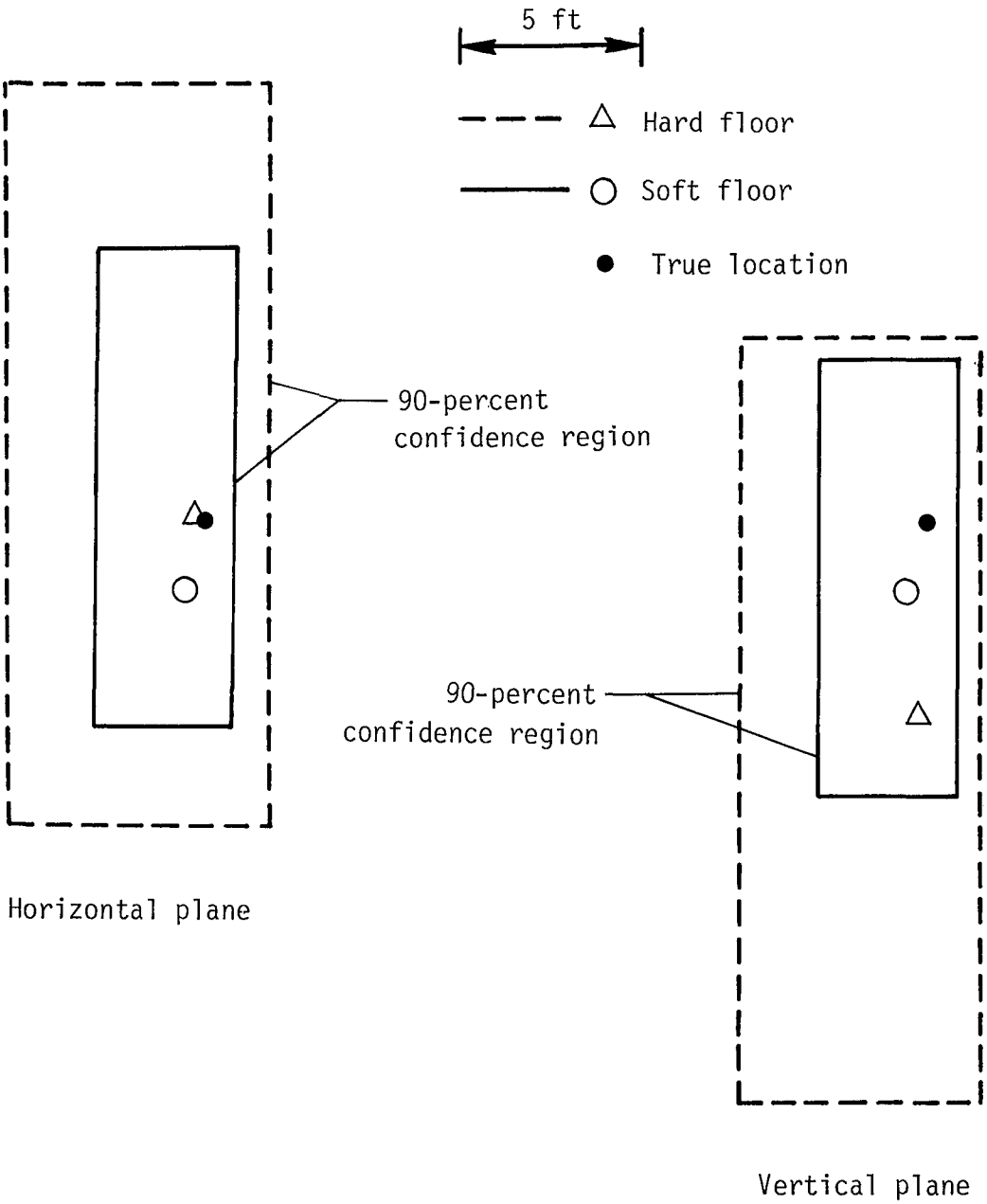

(b) Source position 2.

Figure 18.- Continued.

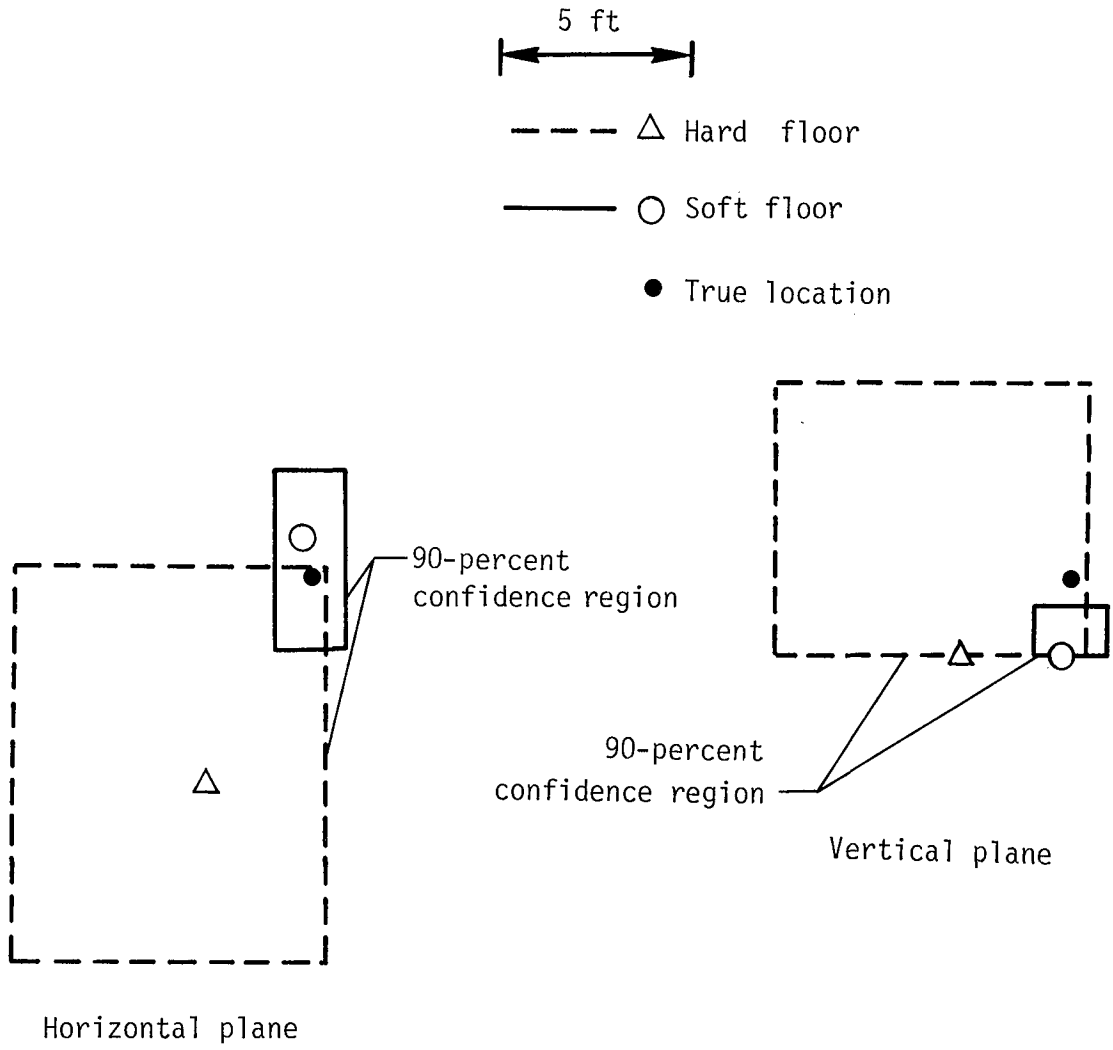

(c) Source position 3.

Figure 18.- Continued.

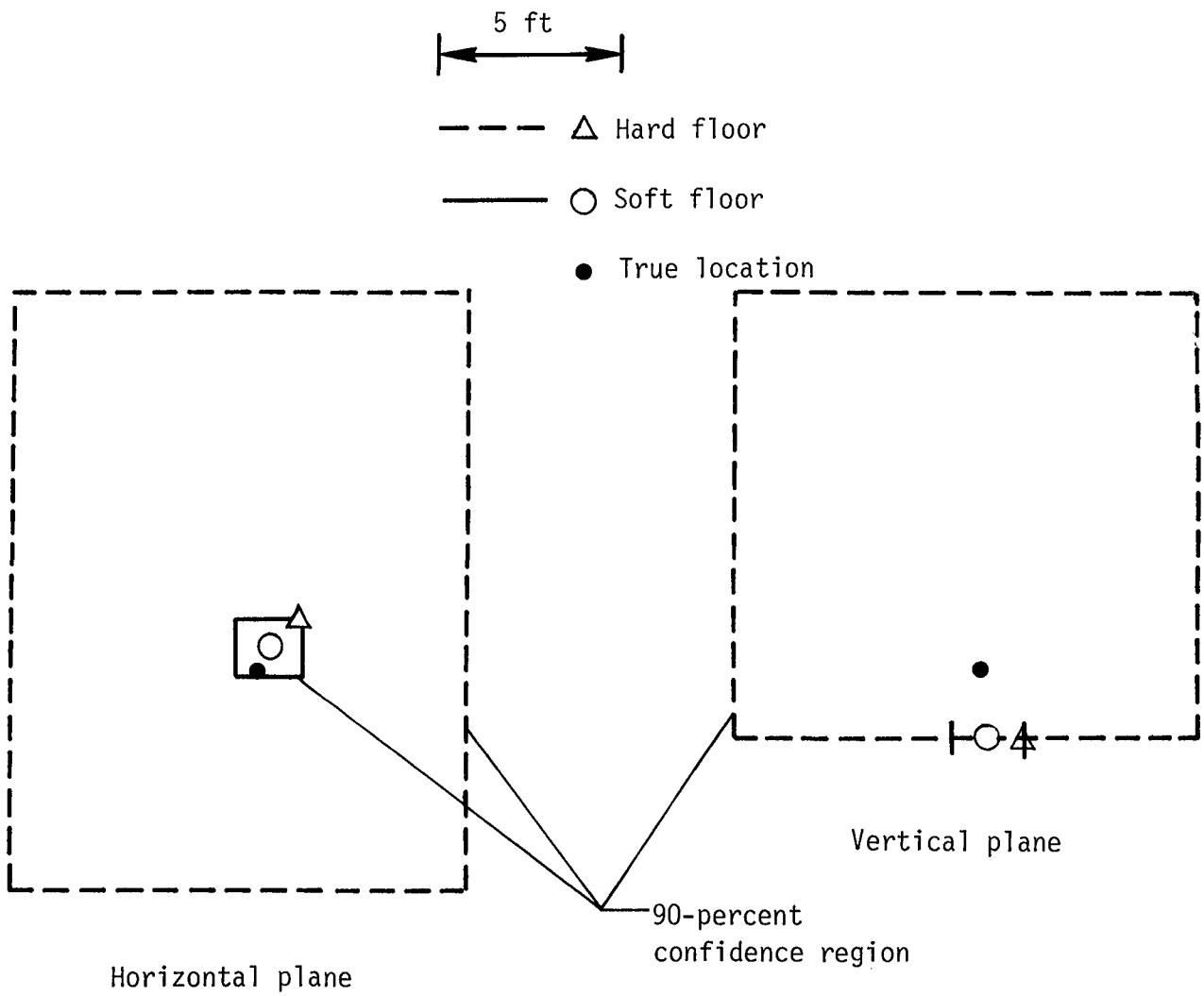

(d) Source position 4.

Figure 18.- Concluded.

1. Report No.	2. Government Accession No.	3. Recipient's Catalog No.
NASA TP-2505		

4. Title and Subtitle	5. Report Date
Location of Noise Sources Using a Phase-Slope Method	November 1985
	6. Performing Organization Code: 505-31-33-13

7. Author(s)	8. Performing Organization Report No.
Richard DeLoach and John S. Preisser	L-15793
	10. Work Unit No.

9. Performing Organization Name and Address	11. Contract or Grant No.
NASA Langley Research Center Hampton, VA 23665-5225	
	13. Type of Report and Period Covered: Technical Paper

12. Sponsoring Agency Name and Address	14. Sponsoring Agency Code
National Aeronautics and Space Administration Washington, DC 20546-0001	

15. Supplementary Notes

16. Abstract

Two three-element microphone arrays have been used to predict the position of both pure-tone and broadband noise sources in an anechoic chamber under different ground impedance conditions. Source positions were predicted using the slope of phase-frequency plots between array elements. A phase-slope method for quantitatively assessing both the accuracy and precision of estimates of noise source location has been introduced and illustrated. When the phase-slope method was used, there was higher accuracy and more precision in estimates of source location with a small ground impedance than with a large ground impedance. As would be expected, ground impedance effects are larger for low elevation angles than for high elevation angles.

17. Key Words (Suggested by Author(s))

Array
Source location
Phase
Acoustics
Microphones

18. Distribution Statement

Unclassified - Unlimited

Subject Category 71

19. Security Classif. (of this report)	20. Security Classif. (of this page)	21. No. of Pages	22. Price
Unclassified	Unclassified	47	A03

For sale by the National Technical Information Service, Springfield, Virginia 22161

NASA-Langley, 1985

National Aeronautics and
Space Administration
Code NIT-3

Washington, D.C.
20546-0001